iScience

CellPress

Article

von Hippel-Lindau Protein Maintains Metabolic Balance to Regulate the Survival of Naive B Lymphocytes

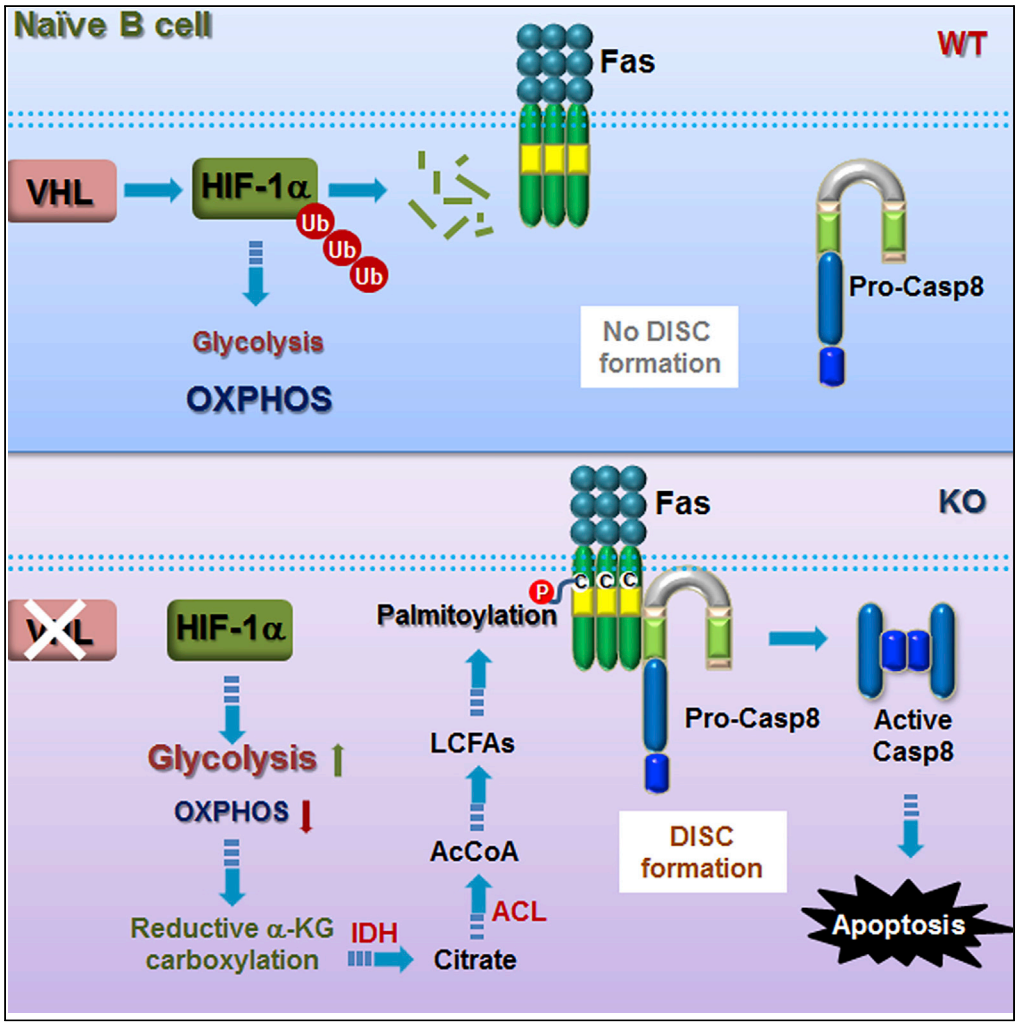

Shengli Xu, Jianxin Huo, Yuhan Huang, ..., Alison Lee, Xijun Ou, Kong-Peng Lam

xu_shengli@bti.a-star.edu.sg (S.X.)
lam_kong_peng@bti.a-star.edu.sg (K.-P.L.)

HIGHLIGHTS

vHL ablation in naive B cells leads to diminishment of mature B cell populations

B cells lacking vHL manifest perturbed metabolism and impaired survival

vHL deficiency in B cells triggers reductive carboxylation of α-KG

Metabolic rewiring in vHL-deficient naive B cells causes caspase-8 activation

Xu et al., iScience 17, 379–392
July 26, 2019
https://doi.org/10.1016/j.isci.2019.07.002

iScience

CellPress

Article

von Hippel-Lindau Protein Maintains Metabolic Balance to Regulate the Survival of Naive B Lymphocytes

Shengli Xu,[1,2,6,*] Jianxin Huo,[1,6] Yuhan Huang,[1] Melissa Aw,[1] Shuwen Chen,[1] Shiya Mak,[1] Lian Yee Yip,[1] Ying Swan Ho,[1] Sze Wai Ng,[1] Andy Hee-Meng Tan,[1] Alison Lee,[1] Xijun Ou,[5] and Kong-Peng Lam[1,3,4,7,*]

SUMMARY

B lymphocytes undergo metabolic reprogramming upon activation to meet the bioenergetic demands for proliferation and differentiation. Yet, little is known if and how the fate of naive B cells is metabolically regulated. Here, we specifically delete von Hippel-Lindau protein (VHL) in B cells using CD19-Cre and demonstrate that metabolic balance is essential for naive B cell survival. Loss of VHL disturbs glycolytic and oxidative metabolic balance and causes severe reduction in mature B cells. Mechanistically, the metabolic imbalance in VHL-deficient B cells, arising from over-stabilization of hypoxia-inducible factor-1α (HIF-1α), triggers reductive glutamine metabolism leading to increased Fas palmitoylation and caspase-8-mediated apoptosis. Blockade of reductive glutamine metabolic flux by lactate supplementation and ATP citrate lyase inhibition restores the metabolic balance and rectifies the impaired survival of VHL-deficient B cells. Hence, we unravel that the VHL/HIF-1α pathway is required to maintain the metabolic balance of naive B cells and ensure their survival.

INTRODUCTION

B lymphocytes develop from committed hematopoietic stem cells in the bone marrow (BM) and populate peripheral lymphoid organs as naive B cells. Upon activation by foreign antigens, naive B cells undergo intensive clonal expansion and differentiate into memory B and antibody-secreting plasma cells that provide an individual with lifelong humoral immunity (Rajewsky, 1996; Goodnow et al., 2010). Recent studies demonstrate that B cells undertake metabolic reprogramming upon activation to meet the bioenergetic demands for proliferation and differentiation (Boothby and Rickert, 2017; Olenchock et al., 2017). Upon B cell receptor cross-linking or stimulation with interleukin-4 or lipopolysaccharide (LPS) *in vitro*, glucose uptake and glycolysis are rapidly increased in B cells (Doughty et al., 2006; Dufort et al., 2007; Caro-Maldonado et al., 2014). Concurrently, glucose oxidation is increased in the activated B cells (Caro-Maldonado et al., 2014). When B cells are stimulated by proteinaceous antigens and differentiate into germinal center (GC) B cells *in vivo*, both glucose uptake and mitochondrial biogenesis are increased (Jellusova et al., 2017). This indicates that activated B cells undergo a balanced glycolytic and oxidative metabolic reprogramming, which differs from the disproportionally increased glycolytic metabolism in activated T cells (Wang et al., 2011). However, it remains unclear if and how metabolism affects the fate of quiescent naive B cells.

Hypoxia-inducible factor 1 (HIF-1) is a basic-helix-loop-helix transcription factor that regulates the expression of genes involved in metabolism and adaption to low oxygen stress. HIF-1 plays multifaceted roles in innate and adaptive immunity (Palazon et al., 2014). It is important for neutrophil survival and bactericidal activity of macrophages (Cramer et al., 2003) and essential for regulating glycolysis in $CD4^+$ T cells and Th17 cell differentiation (Shi et al., 2011; Dang et al., 2011). HIF-1 is heterodimeric and comprises an inducibly expressed oxygen-sensitive α subunit and a constitutively expressed β subunit. Its activity is largely determined by protein stability of the α subunit. Under normoxia, HIF-1α is hydroxylated at specific proline residues and associates with von Hippel-Lindau tumor suppressor protein (VHL), which is the substrate recognition subunit of an E3 ubiquitin-protein ligase, and subsequently ubiquitinated and degraded (Semenza, 2001). Loss of VHL leads to constitutive stabilization of HIF-1α and upregulation of HIF-1's target genes even under normoxia. Mutations in *vhl* gene are found in patients with von Hippel-Lindau disease and in various spontaneous renal cell carcinomas (RCCs) (Gallou et al., 1999; Lemm et al., 1999).

[1]Bioprocessing Technology Institute, Agency for Science, Technology and Research, 20 Biopolis Way, #06-01 Centros, Singapore 138668, Singapore

[2]Department of Physiology, Yong Loo Lin School of Medicine, National University of Singapore, Singapore 117559, Singapore

[3]Department of Microbiology and Immunology, Yong Loo Lin School of Medicine, National University of Singapore, Singapore 117559, Singapore

[4]Department of Pediatrics, Yong Loo Lin School of Medicine, National University of Singapore, Singapore 117559, Singapore

[5]Southern University of Science and Technology, Shenzhen 518055, China

[6]These authors contributed equally

[7]Lead Contact

*Correspondence: xu_shengli@bti.a-star.edu.sg (S.X.), lam_kong_peng@bti.a-star.edu.sg (K.-P.L.)

https://doi.org/10.1016/j.isci.2019.07.002

Deletion of VHL disturbs cellular metabolism and affects activation and differentiation of various immune cells. For example, deletion of VHL in Treg cells results in their acquiring Th1-like inflammatory properties with excessive interferon-γ production due to augmented glycolysis (Lee et al., 2015). VHL deficiency in $CD8^+$ T cells enhances their effector response against chronic infection and tumor growth by averting T cell exhaustion (Doedens et al., 2013). Recent studies showed that HIF-1 over-stabilization by VHL deletion inhibits activation-induced deaminase expression and mTORC1 activation and compromises B cell differentiation in GC (Abbott et al., 2016; Cho et al., 2016), suggesting that VHL is important for B cell activation.

Here, we investigate VHL's role in naive B cells, in which *Vhl* is specifically deleted in B cells using CD19-Cre. We show that VHL ablation causes imbalanced glycolytic and oxidative metabolism in quiescent naive B cells and leads to reduced mature B cell populations. Strikingly, VHL-deficient B cells manifest augmented caspase-8-dependent apoptosis. The metabolism and survival defects of VHL-deficient B cells are largely due to HIF-1α over-stabilization and could be rectified by its deletion. We further demonstrate that the metabolic imbalance in naive VHL-deficient B cells triggers reductive glutamine metabolism, causing constitutive Fas palmitoylation and caspase-8 activation. These data suggest that the VHL-HIF-1α pathway is important for the survival of naive B cells by maintaining metabolic balance and restraining caspase-8 activation.

RESULTS

Reduced Mature B Cell Populations in VHL-Deficient Mice

To investigate the role of VHL in naive B cells, we crossed mice bearing *loxP*-flanked (floxed) *Vhl* alleles with $Cd19^{Cre/+}$ mice, which express Cre recombinase specifically in B cells, to generate $Vhl^{fl/fl}Cd19^{Cre/+}$ (VHL-deficient) mice. These mice were grossly normal and had no obvious phenotype when compared with wild-type $Vhl^{+/+}Cd19^{Cre/+}$ (WT) mice. Quantitative reverse-transcriptase PCR revealed that *Vhl* mRNA was significantly decreased in splenic B cells of VHL-deficient compared with control mice (Figure S1A). Immunoblotting further showed barely detectable VHL but markedly increased HIF-1α protein in VHL-deficient compared with WT B cells (Figure S1B). The level of HIF-2α, which can be targeted by VHL, was also elevated in VHL-deficient splenic B cells. These results suggest that VHL is efficiently deleted and HIF proteins are accumulated in mutant B cells.

Next, we assessed if VHL deficiency would perturb B cell development in the BM of VHL-deficient mice, as B cell development was impaired in the BM of HIF-1α-deficient RAG2 chimeric mice (Kojima et al., 2002). Flow cytometric analysis revealed that the total cellularity of BM and the frequency and absolute number of $IgM^+IgD^{low/-}$ immature B cells, which are c-kit^- and correspond to Hardy fraction E (data not shown), are normal in VHL-deficient mice (Figures S1C and S1D left, Figures 1A and 1B left). In contrast, the population of IgM^+IgD^{high} mature B cells, which are c-kit^- and correspond to Hardy fraction F (data not shown), was significantly reduced in VHL-deficient mice (Figure S1D right, Figures 1A and 1B right). However, VHL-deficient and WT mice had comparable $IgM^-IgD^-B220^+CD43^+$ pro-B and $IgM^-IgD^-B220^+CD43^-$ pre-B cell populations (Figures S1E–S1G), which are c-kit^+ and correspond to Hardy fractions A–C and fraction D, respectively (data not shown). Although it is not clear whether VHL is important for early B cell populations, due to apparently less efficient CD19-Cre-mediated *Vhl* deletion in these cells (50%–65%) compared with the deletion in mature B cells (>75%) (Figure S1H) and the considerable amount of VHL proteins present in these cells (Figure S1I), our results clearly suggest that VHL is required for mature B cells in the BM.

In the spleen and lymph nodes, the frequency and number of $B220^+IgM^+$ total B cells were significantly decreased in VHL-deficient compared with WT mice (Figures 1C and 1D). Moreover, the total cellularity of spleen was also reduced in VHL-deficient mice (Figure S1J). The defect was equally evident by histological analysis, as splenic B cell (IgD^+) follicles were smaller in VHL-deficient than WT mice (Figure 1E and data not shown). However, the positioning of B cells, T cells, $CD169^+$ marginal metallophilic macrophages (Figure 1E), and IgM^{high} marginal zone B cells (Figure S2A) was unaffected in the spleen of VHL-deficient mice. The frequencies of $B220^+CD93^-CD23^+CD21^{lo}$ follicular and $B220^+CD93^-CD23^-CD21^+$ marginal zone B cells within the $B220^+CD93^-$ mature B cell compartment were also comparable between VHL-deficient and WT mice (Figure S2B), suggesting that VHL deficiency causes a general reduction in all B cell populations rather than in a specific B cell subset. Also, the frequency of $B220^+CD19^+$ B cells in peritoneal cavities were reduced by ~3-fold in VHL-deficient compared with WT mice (Figure 1F), although the relative abundancies of

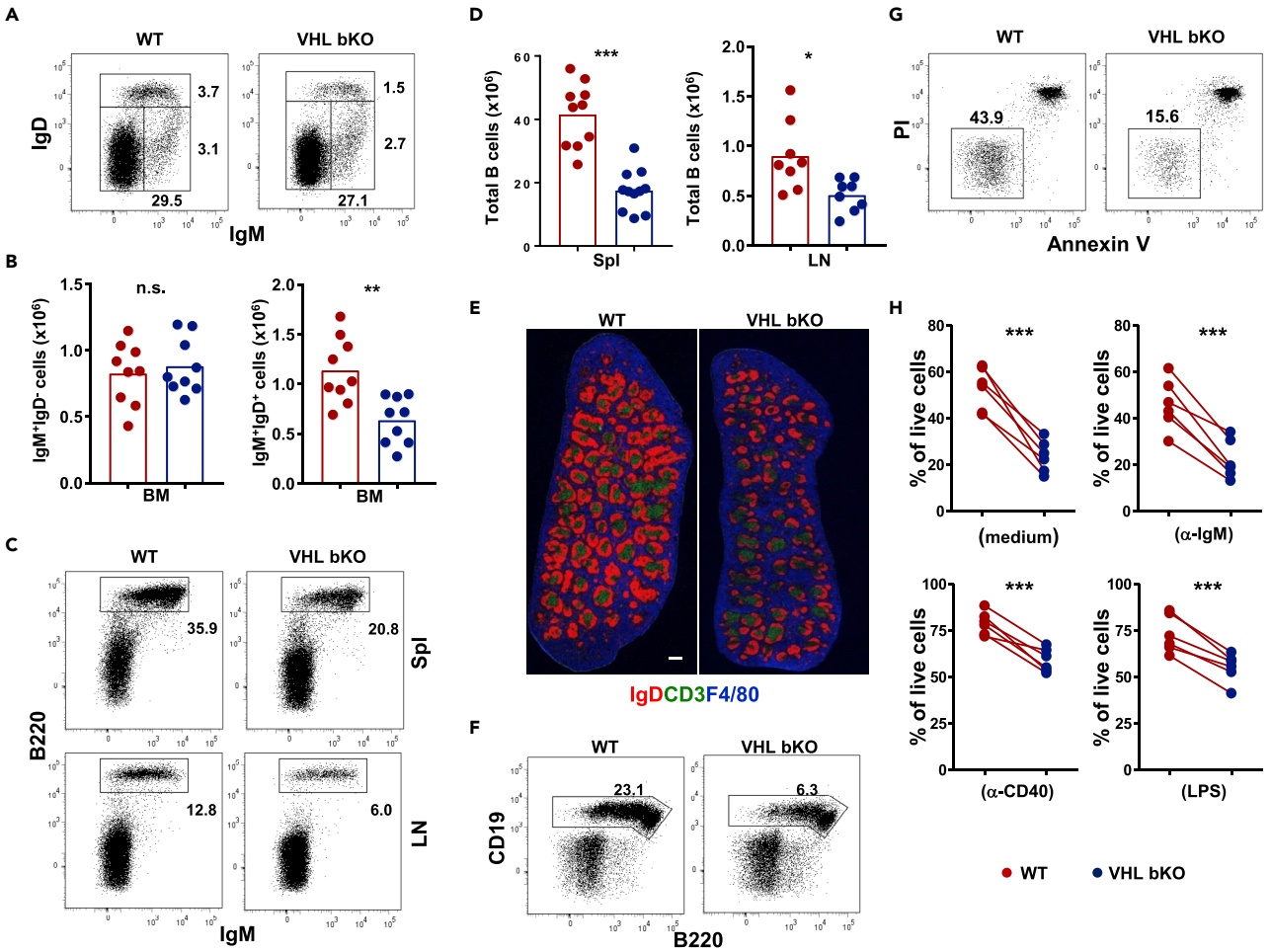

Figure 1. Reduced Mature B Cell Populations in VHL-Deficient Mice

(A, C, and F) Flow cytometric analysis of B cells in various lymphoid organs of WT and VHL-deficient mice. Numbers adjacent to outline areas indicate the percentage of gated cells over total cells in the BM (A), spleen (Spl) (C, upper panel), inguinal lymph nodes (LN) (C, lower panel), and peritoneal cavities (F).

(B and D) Enumeration of B cells in various lymphoid organs of WT and VHL-deficient mice. Number of IgM^+IgD^- immature and IgM^+IgD^+ mature B cells in the BM (B) and total IgM^+B220^+ B cells in the spleen and lymph nodes (D) of WT (red) and VHL-deficient (blue) mice was calculated based on total cell count and their percentage as determined by flow cytometry.

(E) Microscopy of spleen sections of unchallenged WT and VHL-deficient mice. B cell follicles (red), T cell zones (green), and red pulps (blue) were stained with anti-IgD, anti-CD3, and F4/80 antibodies, respectively. Scale bar, 500 μm.

(G) Flow cytometric analysis of B cell survival *in vitro*. WT and VHL-deficient B cells were cultured for 16 h and analyzed by flow cytometry for Annexin V and propidium iodide (PI) staining.

(H) Percentage of PI^- Annexin V^- live B cells in different cultures. B cells were cultured in medium alone or in the presence of anti-IgM (20 μg/mL) or anti-CD40 (1 μg/mL) antibodies or LPS (100 ng/mL) for 16 h and examined by flow cytometry. Each symbol represents one mouse, and the height of bars indicates the mean.

Data shown are representative of more than five independent experiments (A, n = 9; C, n = 10 for spleen and n = 8 for lymph nodes; E, n = 5; F, n = 8; and G, n = 6). n.s., not significant; *$p < 0.05$, **$p < 0.01$, ***$p < 0.001$ (Student's t test). See also Figure S1.

conventional B2 and B1 B cell subsets within the total B cell population of peritoneal cavities were comparable between VHL-deficient and WT mice (data not shown). In addition, the percentage and total number of T cells in the spleen and lymph nodes were comparable between VHL-deficient and WT mice (data not shown). Together, these data suggest that VHL deficiency diminishes naive B cell populations.

Impaired Survival of VHL-Deficient B Cells

It is possible that the reduced naive VHL-deficient B cell populations was due to defective proliferation caused by accumulation of HIF-1α, which was showed to influence cell-cycle arrest of hypoxic B cells

(Goda et al., 2003). However, the percentage of Ki-67$^+$ proliferating B cells in spleens of unchallenged VHL-deficient and WT mice was found to be similar (Figure S3A). The live carboxyfluorescein succinimidyl ester (CFSE)-labeled VHL-deficient B cells also formed blasts, as envisaged in the forward scatter/side scatter (FSC/SSC) profiles (data not shown), and underwent equivalent cell divisions compared with WT B cells upon stimulation with anti-IgM antibody or LPS (Figure S3B). Moreover, the levels of activation markers, such as CD25, CD69, CD86, and major histocompatibility complex II, in the *ex vivo* naive or *in vitro* stimulated VHL-deficient and WT B cells were comparable (Figures S3C and S3D). Conversely, the survival of VHL-deficient B cell was drastically impaired, as the percentage of Annexin V$^-$PI$^-$ live VHL-deficient B cells was ~3-fold lower than that of WT B cells (Figures 1G and 1H upper left), whereas the percentage of PI$^+$Annexin V$^+$ VHL B KO cells was significantly higher that of WT cells (83.8% $\pm$ 2.6% versus 55.2% $\pm$ 3.8%; $p < 0.001$) after overnight culture. Besides, the exacerbated cell death of VHL-deficient cells could not be rescued by treatment with anti-IgM antibodies, anti-CD40 antibodies, or LPS (Figure 1H). These data suggest that VHL is important for the survival but not the proliferation or activation of naive B cells.

Loss of VHL Perturbs Glycolytic and Oxidative Metabolism Balance in Naive B Cells

Next, we investigated how VHL deficiency impaired naive B cell homeostasis by comparing the gene expression profiles of VHL-deficient and WT B cells. Microarray study revealed 155 genes to be differentially expressed in the two cell populations (Figure 2A and Table S1), with 141 genes (90%) significantly upregulated in mutant B cells. Gene set enrichment analysis further revealed that 29 of the 50 HIF-1α target genes were significantly upregulated in VHL-deficient cells (Figures 2B and 2C), consistent with their augmented expression of HIF-1α protein. Expression of HIF-2α target genes were also increased in VHL-deficient cells (Figure 2C), correlating with increased HIF-2α protein in these cells (Figure S1B). Notably, genes encoding glycolysis enzymes were significantly upregulated in VHL-deficient cells, including hexokinase (HK) 1, HK2, phosphofructokinase liver type, phosphofructokinase platelet and 6-phosphofructo-2-kinase/fructose-2,6-biphosphatase 2, fructose bisphosphate aldolase, glyceraldehyde-3-phosphate dehydrogenase, phosphoglycerate mutase, enolase-1, pyruvate kinase M, and lactate dehydrogenase α (LDHα) (Figure 2D). Immunoblotting further confirmed the enhanced expression of these enzymes in naive VHL-deficient compared with WT B cells (Figures 2E and S7).

The increased mRNA levels of glycolytic enzyme genes and protein levels of these enzymes in VHL-deficient B cells would suggest that the overall enzymatic activity was augmented due to the increased amount of enzymes, although we did not directly measure the enzymatic activities of these enzymes. Consistent with the enhanced levels of glycolytic enzymes, VHL-deficient B cells manifested increased extracellular acidification rate (ECAR), a surrogate for glycolysis, in response to glucose (Figures 2F and 2G), and produced much more lactate compared with WT cells (Figure 2H), indicating enhanced glycolysis in the mutant cells. This is similar to situations wherein much more enhanced glycolysis in Th17 cells than Treg cells and VHL-deficient CD8$^+$ T cells than WT CD8$^+$ T cells were demonstrated to be consistent with the increased HIF-1a protein level and the mRNA levels of genes encoding various glycolytic enzymes in Th17 and VHL-deficient CD8$^+$ T cells (Shi et al., 2011; Doedens et al., 2013). However, VHL-deficient B cells exhibited reduced basal mitochondrial oxygen consumption rate (OCR), which is reflective of oxidative phosphorylation (OXPHOS), and spare respiratory capacity (SRC) as indicated by the difference between basal OCR and maximal OCR achieved after adding oligomycin and the ionophore FCCP (Figures 2I and 2J). These data suggest that VHL deficiency causes imbalanced glycolytic and oxidative metabolism in naive B cells.

Removal of HIF-1α Rectifies Metabolic and Survival Defects of VHL-Deficient B Cells

We next asked if the defects of VHL-deficient B cells were due to HIF-1α-accumulation. We generated *Hif-1α*$^{fl/fl}$*Cd19*$^{Cre/+}$ and *Vhl*$^{fl/fl}$ *Hif-1α*$^{fl/fl}$*Cd19*$^{Cre/+}$ mice (denoted as HIF-1α bKO and dbKO mice, respectively) and compared them with VHL-deficient and WT mice. Removal of HIf-1α did not affect naive B cells as the percentage and total number of B cells in the spleen and lymph nodes were equivalent between HIF-1α bKO and WT mice (Figures 3A and 3B). However, ablating HIF-1α almost completely restored the diminished B cell compartment in VHL-deficient B mice, as both the percentage and number of B cells were comparable between dbKO and WT mice. Immunoblotting confirmed that HIF-1α accumulation in VHL-deficient B cells was obliterated in dbKO B cells (Figure 3C). Interestingly, dbKO B cells survived much better than VHL-deficient cells and as normal as WT B cells (Figure 3D). Also, different from the VHL-deficient B cells, which had distorted glycolytic and oxidative metabolisms, the dbKO B cells exhibited normal ECAR and OCR profiles, same as WT cells (Figures 3E and 3F). These findings suggest that the survival and metabolic defects of VHL-deficient B cells are due to HIF-1α over-accumulation.

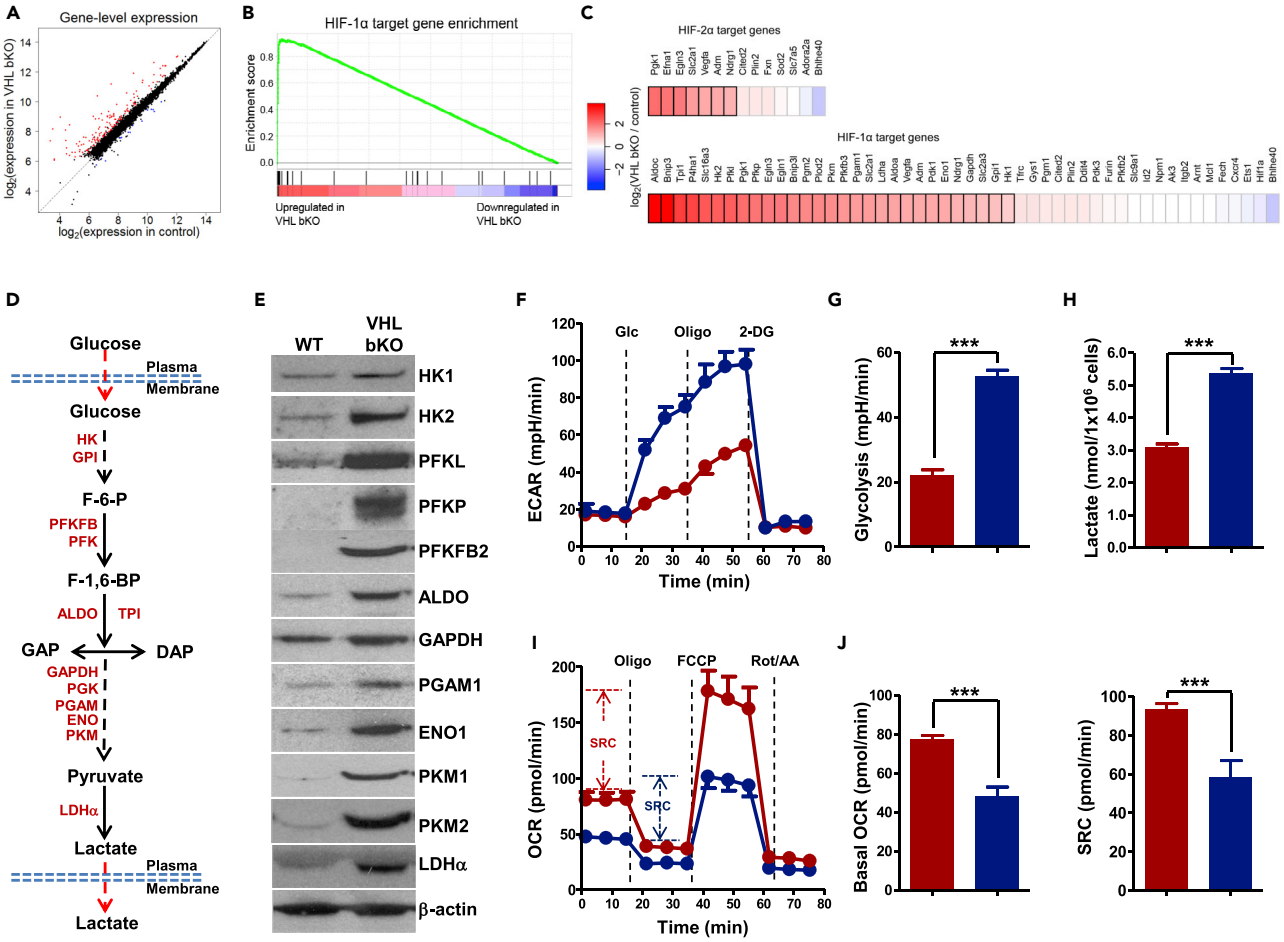

Figure 2. Imbalanced Glycolytic and Oxidative Metabolisms in VHL-Deficient B Cells

(A) Scatterplot of gene expression of microarray analysis of VHL-deficient and WT B cells. Genes significantly upregulated (fold-change > 1.5, $p < 0.05$) and downregulated (fold-change < −1.5, $p < 0.05$) were shown in red and blue, respectively.

(B) Gene set enrichment analysis (GSEA) enrichment curve of HIF-1α target genes in VHL-deficient B cells (enrichment score [ES] = 0.927, normalized ES = 2.41, false discovery rate q value < 0.01). Vertical black lines indicate HIF-1α target genes detected by microarray analysis.

(C) Heatmap depicting $\log_2$ fold change of expression of HIF-1α and HIF-2α target genes in VHL-deficient versus WT B cells. Genes that were identified as differentially expressed with statistical significance were indicated with a black border.

(D) Schematic of glycolytic pathway.

(E) Immunoblotting of glycolytic enzymes in VHL-deficient and WT B cells. β-Actin was used as the loading control.

(F and G) Analysis of extracellular acidification rate (ECAR) in VHL-deficient (blue) and WT (red) B cells. Real-time changes in ECAR of B cells with the addition of glucose (Glc) (10 mM), oligomycin (Oligo) (1.0 μM), and 2-deoxy-D-glucose (*2*-DG) (50 mM) was measured (F). Basal glycolysis was quantified as the difference of ECAR before and after addition of glucose (G).

(H) Quantification of lactate produced by B cells. The amount of lactate in the supernatant of equal number of VHL-deficient and WT B cells cultured for 1 h was quantified.

(I) Oxygen consumption rate (OCR) in VHL-deficient and WT B cells. OCR of B cells with the addition of oligomycin (Oligo) (1.0 μM), FCCP (1.0 μM), and rotenone plus antimycin (Rot/AA) (0.5 μM for each) was measured in real time. Spare respiratory capacity (SRC) is indicated as the difference between basal OCR and maximum OCR after addition of FCCP.

(J) Quantification of basal OCR (leaf panel) and SRC (right panel) in VHL-deficient and WT B cells. Bar graphs represent mean ± SD (n = 5 for G and J; n = 3 for H). Data shown are representative of more than 3 experiments (E, n = 3; F and I, n = 5). For F and I, each data point represents mean ± SD, n = 5. ***$p < 0.001$ (Student's t test). See also Figures S2 and S7.

VHL-Deficient B Cells Manifest Caspase-8-Dependent Apoptosis

Albeit the survival and metabolic defects in VHL-deficient B cells were rescued by HIF-1α-deletion, the mechanism whereby HIF-1α over-accumulation impairs naive B cell survival was unclear. Apparently, VHL-deficient B cells had higher expression of *bnip3*, which encodes atypical BH3-only proteins BNIP3 (Figure S4A and Table S1), and its upregulation was HIF-1α-dependent as its protein level was markedly reduced in dbKO

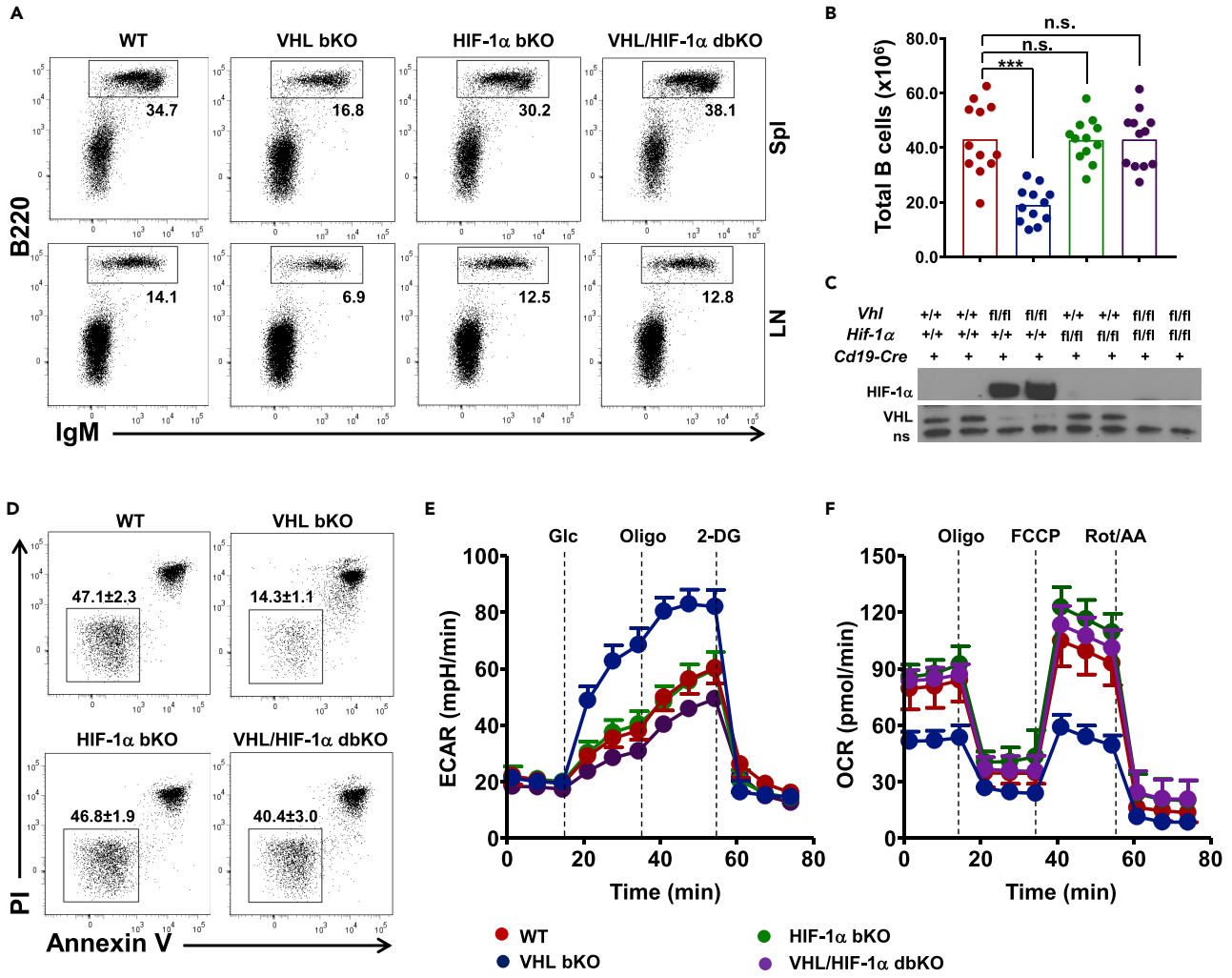

Figure 3. Over-accumulation of HIF-1α Underlies Survival Defect and Distorted Metabolism in VHL-Deficient B Cells

(A) Flow cytometric analysis of B cells in the spleen and lymph nodes of WT, VHL-deficient, HIF-1α bKO, and VHL/HIF-1α bdKO mice. Numbers adjacent to the outline areas indicate percentage of gated cells over total cells.

(B) Enumeration of total splenic B cells in mice of various genotypes. Each symbol represents one mouse, and the height of bars indicates the mean.

(C) Immunoblotting of HIF-1α and VHL in B cells of different genotypes as indicated. A non-specific (ns) band served as loading control.

(D) Flow cytometric analysis of the survival VHL/HIF-1α bdKO B cells. Splenic B cells were cultured in medium for 16 h and analyzed for Annexin V and propidium iodide (PI) staining. Numbers adjacent to outline areas indicate the percentage of PI^{-}Annexin V^{-} live B cells (mean ± SD, n = 5).

(E and F) ECAR and OCR analyses of B cells. ECAR (E) and OCR (F) of splenic B cells from mice of various genotypes were measured in real time with the addition of different compounds as indicated.

Data are representative of 12 (A), 3 (C), or 5 (D, E, and F) experiments. For E and F, each data point represents mean ± SD, n = 5. n.s., not significant; ***$p < 0.001$ (Student's t test). See also Figure S3.

B cells (Figure S4B). BNIP3 has been known to be involved in cell death induced by hypoxic injury such as ischemia (Hamacher-Brady et al., 2007; Schmidt-Kastner et al., 2004) and regulate opening of mitochondrial permeability transition pore (mPTP) to induce necrosis or caspase-9-dependent apoptosis (Chinnadurai et al., 2008; Gustafsson, 2011). BNIP3 was also shown to promote survival and memory formation of natural killer cells (O'Sullivan et al., 2015). However, the mPTP opening was not affected in VHL-deficient B cells despite the upregulated BNIP3 (Figure S4C). Treatment of VHL-deficient B cells with mPTP inhibitors, bongkrekic acid or 2-aminoethoxydiphenyl borate, had no effect on their survival (Figure S4D). Also, no enhanced caspase-9 activation was found in VHL-deficient cells (Figure S4E). These data suggest that the impaired survival of VHL-deficient B cells is not likely due to BNIP3 upregulation. However, compared with WT cells, VHL-deficient B cells exhibited enhanced caspase-3 activation, which was evident after 2 h and became more

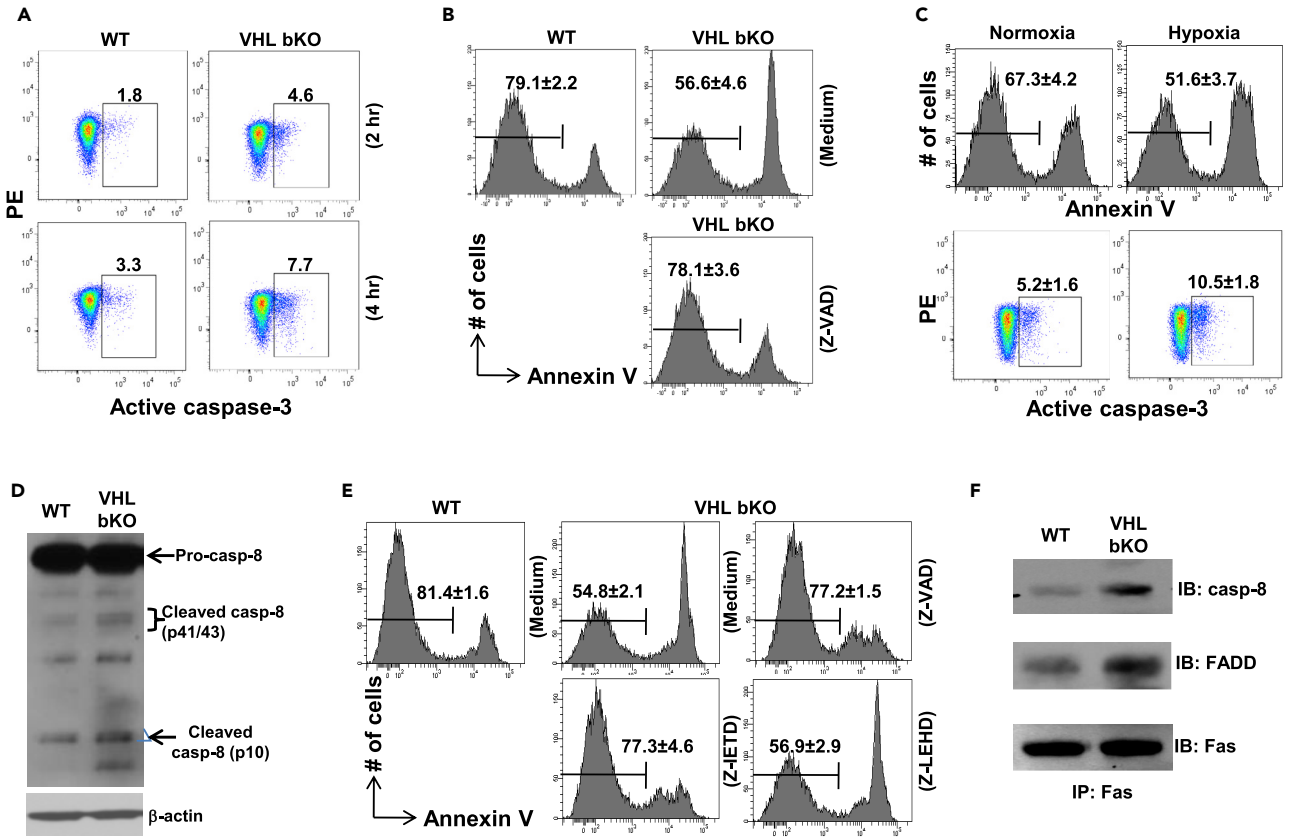

Figure 4. VHL-Deficient B Cells Exhibit Exacerbated Caspase-8 Activation

(A) Flow cytometric detection of caspase-3 activation in VHL-deficient B cells. VHL-deficient and WT B cells were cultured for 2 or 4 h and stained for activated caspase-3.

(B) Survival of VHL-deficient B cells after treatment with pan-caspase inhibitor Z-VAD. VHL-deficient B cells were cultured in medium alone or in the presence of Z-VAD (10μM) for 8 h followed by flow cytometry to detect Annexin V^- live cells. Numbers indicate percentage of Annexin V^- live cells (mean ± SD, n = 5).

(C) Survival and caspase-3 activation in B cells under normoxia and hypoxia. WT B cells were cultured under normoxia (21% O_2) or hypoxia (1% O_2) for 16 h followed by flow cytometry to detect Annexin V^- live cells and caspase-3 activation. Numbers indicate percentage of Annexin V^- live cells (upper panel, mean ± SD, n = 5) or activated caspase-3^+ cells (lower panel, mean ± SD, n = 5).

(D) Immunoblotting of caspase-8 activation in VHL-deficient B cells. Whole-cell lysates of VHL-deficient and WT B cells were subjected to immunoblotting to detect pro- and cleaved-caspase-8. β-Actin was used as loading control.

(E) Survival of VHL-deficient B cells after treatment with pan-caspase inhibitor Z-VAD (10μM), caspase-8 inhibitor Z-IETD (10μM) or caspase-9 inhibitor Z-LEHD (10μM) for 8 h. Numbers indicate percentage of Annexin V^- live cells (mean ± SD, n = 5).

(F) DISC formation in VHL-deficient B cells. VHL-deficient and WT B cells were lysed and subjected to immunoprecipitation with anti-Fas antibody. Fas-associated caspase-8 and FADD were detected by immunoblotting subsequently.

Data are representative of 4 (A) or 5 (D, F) experiments. See also Figures S4 and S7.

pronounced after 4 h of normoxic culture (Figure 4A). Addition of pan-caspase inhibitor Z-VAD largely rescued the survival defect of mutant cells (Figure 4B). Interestingly, WT B cells cultured under hypoxia also had increased caspase-3 activation and apoptosis compared with cells under normoxia (Figure 4C). These data suggest that VHL deficiency or hypoxia can trigger caspase-3-dependent apoptosis of naive B cells.

A previous study showed that *Vhl* deletion using Lck-Cre caused enhanced mRNA expression and activity of caspase-8 in thymocytes (Biju et al., 2004). Despite the comparable transcript and protein levels of caspase-8 in WT and VHL-deficient B cells, the amount of cleaved/activated forms of caspase-8 was significantly increased in mutant B cells (Table S1, Figures 4D and S7). In addition, caspase-8 specific inhibitor Z-IETD-fmk largely rescued the survival defect of VHL-deficient cells and to the same extent as the pan-caspase inhibitor Z-VAD (Figure 4E). In contrast, caspase-9 was not activated (Figure S4E) and caspase-9-specific inhibitor Z-LEHD-fmk had no effect on VHL-deficient B cell survival. These data suggest that enhanced caspase-8 activation is responsible for the caspase-3 activation and apoptosis of VHL-deficient B cells.

Caspase-8 activation is initiated when its proenzyme is recruited together with adaptor protein FADD to death receptors, such as Fas, to form death-inducing signaling complex (DISC) which causes its cleavage and activation (Kischkel et al., 1995). Interestingly, B cell-specific deletion of Fas leads to severe autoimmunity in mice, suggesting that Fas is important for the homeostasis of naive B cells despite its minimal expression (Hao et al., 2008). Hence, we examined if Fas-mediated DISC formation was affected in VHL-deficient B cells. Immunoprecipitation assay revealed increasing amount of caspase-8 and FADD associated with Fas in resting VHL-deficient compared with WT B cells (Figure 4F), suggesting a constitutive Fas-mediated DISC formation in the mutant cells.

VHL Deficiency Decouples Glycolysis from TCA and Induces Reductive Carboxylation of α-KG and Fas Palmitoylation in B Cells

Given the distorted metabolism and yet largely normal expression of cell survival genes in VHL-deficient B cells, we next investigated the metabolism of these cells in detail by performing a metabolomic profiling study. We obtained totally ~100 metabolites with confirmed identities in B cells using liquid chromatography-mass spectrometry (LC-MS) (Table S2). Strikingly, VHL-deficient B cells exhibited high levels of various long-chain acylcarnitines (LCACs) (Figure 5A), which are metabolic intermediates of fatty acid (FA) oxidation (FAO). The high level of LCACs could be due to an impaired FAO in VHL-deficient cells. To test this, we treated B cells with etomoxir, an inhibitor of carnitine palmitoyltransferase-1 that is a critical enzyme for FAO, to totally block FAO. The reduction in basal OCR and SRC by etomoxir would reflect the FAO contribution to OCR. Etomoxir caused similar reduction in basal OCR and SRC levels in VHL-deficient and WT B cells (Figure S5A), and percent reduction was even slightly more in mutant B cells (Figure S5B), suggesting that LCACs' accumulation in mutant cells was not ascribed to an impaired FAO. It was also not due to enhanced uptake of exogenous triacylglycerol substrates via scavenger receptor CD36 and the subsequent lipolysis by lysosomal acid lipase (LAL) for releasing FAs, as VHL-deficient and WT B cells had comparable CD36 and LAL expression (Figures S5C and S5D) and equivalent amount of acylglycerol species (Table S2).

It is possible that the LCACs' accumulation in mutant B cells was indicative of increased *de novo* FA synthesis. In fact, recent studies showed that VHL-deficient RCC or hypoxic tumor cells had enhanced FA synthesis from glutamine (Mullen et al., 2011; Metallo et al., 2011; Wise et al., 2011; Filipp et al., 2012). In these cells, glucose was mainly converted to lactate and uncoupled from tricarboxylic acid (TCA) cycle, and isocitrate dehydrogenase-mediated reductive carboxylation of glutamine-derived α-ketoglutarate (α-KG) was triggered to fuel citrate production and lipogenesis for cell growth. We postulated that the distorted metabolism in VHL-deficient cells, arising from over-stabilization of HIF-1α, could also uncouple glycolysis from TCA cycle and trigger reductive carboxylic metabolism for lipogenesis. To test this, we first examined the activity of pyruvate dehydrogenase (PDH) that drives hypoxic glycolysis decoupling from TCA cycle and is negatively regulated by PDH kinase isoform 1 (PDK1) (Fendt et al., 2013; Kim et al., 2006), a direct target of HIF-1α. Consistent with the HIF-1α's accumulation, PDK1 expression was enhanced (Figures 5B and S7) and PDH activity was decreased concurrently in VHL-deficient B cells (Figure 5C). Interestingly, whereas glucose slightly increased OCR in WT cells, as they fuel into TCA cycle through pyruvate, glucose addition reduced OCR in VHL-deficient B cells (Figure 5D), indicating that their abnormally enhanced glycolysis could further dampen OXPHOS. These data suggest that glycolysis is indeed decoupled from TCA cycle in the naive mutant B cells.

Compared with WT cells, mutant B cells also had higher α-KG to citrate ratio (Figure 5E), the trigger for reductive carboxylation of α-KG (Fendt et al., 2013). To assess directly the reductive α-KG carboxylation, we performed isotopic ^{13}C-labeling assay by culturing B cells in [$^{13}C_5$,$^{15}N_2$] glutamine-containing medium for 4 h and measuring ^{13}C enrichment in various metabolites by LC-MS. Reductive carboxylation of α-KG would generate mass isotopomers, such as M5 citrate, M3 oxaloacetate, M3 aspartate, M3 malate, and M3 fumarate, from the labeled glutamine (Figure 5F). It was found that the amounts of M5 citrate, M3 malate, M3 fumarate, and M3 aspartate were increased in VHL-deficient compared with WT B cells (Figure 5G), suggesting that mutant B cells have enhanced reductive carboxylation of α-KG.

However, it was still elusive how enhanced reductive α-KG carboxylation was linked to compromised survival of VHL-deficient B cells. Lipogenesis via reductive α-KG carboxylation was engaged to support the growth of tumor cells lacking VHL or under hypoxia, but it is obviously unnecessary for naive B cells as

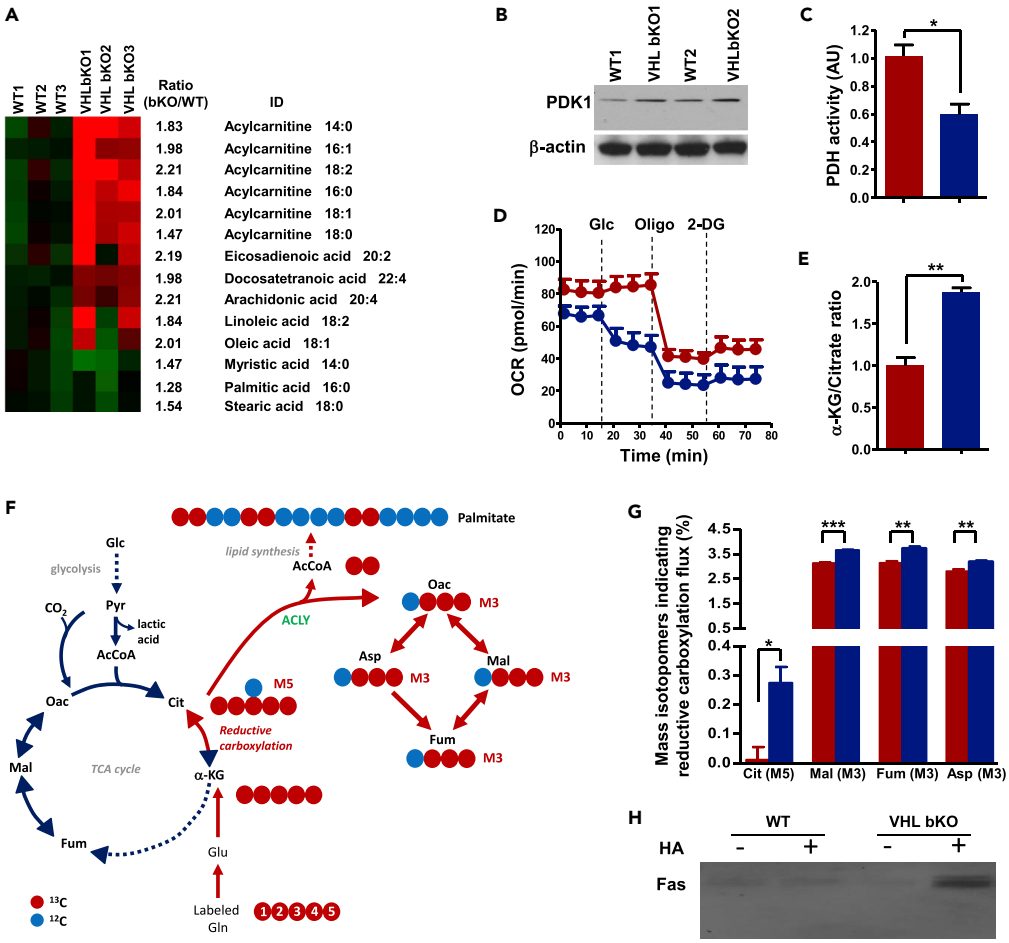

Figure 5. Increased Reductive Carboxylation of α-KG and Constitutive Palmitoylation of Fas in VHL-Deficient B Cells

(A) Heatmap depicting lipid metabolite difference between WT and VHL-deficient (bKO) B cells. Lipid metabolites from bKO and WT B cells were subjected to ultra-performance LC-MS. Data were pre-processed and normalized to total protein concentration in each sample.

(B) Immunoblotting of PDK1 in B cells. Whole-cell lysates from WT and VHL-deficient B cells were subjected to immunoblotting with anti-PDK1 antibody. β-Actin was used as loading control.

(C) PDH activity in VHL-deficient and control B cells. The activity of PDH in VHL-deficient B cells (blue) was measured and presented relative to that in control B cells (red), set as 1.

(D) Real-time changes in OCR of VHL-deficient (blue) and control (red) B cells with the addition of Glc (10 mM), Oligo (1.0 μM), and 2-DG (1.0 μM).

(E) α-Ketoglutarate (α-KG)/citrate ratio in VHL-deficient and control B cells. The ratio in VHL-deficient cells (blue) was presented relative to that in control cells (red), set as 1.

(F) Carbon atom transition map depicting patterns of metabolites derived from [$^{13}C_5$,$^{15}N_2$] glutamine during oxidative (blue arrows) and reductive (red arrows) metabolism. Mass isotopomers for reductive glutamine metabolism detection include M5 citrate (Cit), M3 oxaloacetate (Oac), M3 aspartate (Asp), M3 malate (Mal), and M3 fumarate (Fum) from the labeled glutamine.

(G) Evidence for increased reductive carboxylation in VHL-deficient B cells. VHL-deficient (blue) and control (red) B cells were cultured in medium containing 2 mM [$^{13}C_5$,$^{15}N_2$] glutamine for 4 h and ^{13}C enrichment in various intracellular metabolites was measured by LC-MS.

(H) Measurement of Fas palmitoylation. Whole-cell lysates from WT and VHL-deficient B cells were treated with (+) or without (−) hydroxylamine (HA) followed by biotin moiety replacement for pull down with streptavidin-conjugated agarose beads. The pulled down proteins were subjected to immunoblotting with Fas-specific antibody.

Bar graphs represent mean ± SD (n = 3 for C and E and n = 2 for G). Data are representative of 2 (A, G, and H) and 5 (B and D) experiments. For D, each data point represents mean ± SD, n = 5. *p < 0.05, **p < 0.01; ***p < 0.001 (Student's t test).

See also Figures S5 and S7.

they do not have such metabolic needs. Other than contributing to membrane synthesis, LCFAs can also modify proteins at their cysteine residues (Nadolski and Linder, 2007; James and Olson, 1990). For instance, palmitate, the most abundant FA in the cell, preferentially modifies proteins via palmitoylation (Resh, 2012; Salaun et al., 2010). Interestingly, Fas palmitoylation at membrane-proximal cysteine residues of its cytoplasmic region is known to facilitate DISC formation (Chakrabandhu et al., 2007; Feig et al., 2007). The high level of LCACs including palmitoyl carnitine (Figure 5A) and constitutive DICS formation in VHL-deficient B cells (Figure 4F) prompted us to ask if Fas was constitutively palmitoylated in the mutant cells. We examined Fas palmitoylation by employing a non-radioactive acyl-biotinyl exchange (ABE) assay, in which the S-palmitoyl thioester link was cleaved by hydroxylamine (HA) and subsequently replaced by a biotin moiety for protein pull-down. Fas protein was hardly detectable in both HA-treated and HA-untreated WT samples after ABE reaction, suggesting that Fas is not palmitoylated in these cells (Figure 5H). By contrast, a considerable amount of Fas was detected in HA-treated cell lysates from mutant B cells, indicating constitutive palmitoylation in these cells. Together, these results suggest that the distorted metabolism in VHL-deficient B cells activates reductive α-KG carboxylation for lipogenesis, leading to constitutive Fas palmitoylation.

Blockade of Reductive Carboxylation of α-KG Rescues Survival Defect of VHL-Deficient B Cells

As the distorted metabolism in VHL-deficient B cells triggers reductive α-KG carboxylation causing Fas palmitoylation, we next asked if interference with this metabolic pathway could rectify the survival defect of the mutant cells. Lactate supplementation was shown to reverse reductive glutamine metabolism in cells under hypoxia or with impaired respiration (Fendt et al., 2013), as it shifts the reaction direction of LDH from net synthesis to net consumption of lactate to generate pyruvate (Huckabee, 1956) and increases carbon entry into the TCA cycle via acetyl-CoA (Mintun et al., 2004). Thus, we assessed the effect of lactate supplementation on the metabolism and survival of VHL-deficient B cells. We found that lactate indeed reduced LCAC levels, especially the levels of palmitoyl carnitine (C16:0) and linoelaidyl carnitine (C18:2) (Figure 6A), and rectified the elevated ECAR and decreased OCR in VHL-deficient B cells (Figure S6). More interestingly, lactate greatly improved VHL-deficient B cell survival (Figures 6B and 6D). Consistently, caspase-3 activation was significantly reduced by lactate (Figures 6C and 6D), suggesting that blockade of reductive carboxylation of α-KG corrects the metabolic and survival defects in VHL-deficient B cells.

We also evaluated the effect of inhibiting ATP-citrate lyase (ACLY), another critical metabolic enzyme along the reductive glutamine metabolism pathway, on VHL-deficient B cell survival. We found that SB204990, a specific ACLY inhibitor, significantly rescued the survival defect and dampened caspase-3 activation in mutant B cells (Figures 6B–6D). Notably, combinatory treatment with lactate and SB204990 had more profound rescuing effect on VHL-deficient cells than individual treatment (Figures 6B–6D). The constitutive DISC formation and caspase-8 activation in VHL-deficient B cells were also significantly reduced by the combinatory treatment (Figure 6E). These data suggest that enhanced caspase-8-dependent apoptosis of VHL-deficient B cells is largely due to increased reductive carboxylation of α-KG arising from the distorted metabolism.

DISCUSSION

In this study, we uncover an important mechanism whereby the survival of naive B cells is metabolically regulated. We demonstrate that VHL deletion in B cells causes over-stabilization of HIF-1α, which leads to imbalanced glycolytic and oxidative metabolism and diminishment of mature B cell. The distorted metabolism decouples glucose-derived pyruvate from entering the TCA cycle and triggered reductive glutamine metabolism in the quiescent mutant B cells. The abnormally activated reductive glutamine metabolism triggers increased lipogenesis that causes Fas palmitoylation and constitutive activation of caspase-8, leading to increased apoptosis of VHL-deficient B cells.

A recent study shows that glucose fluxing via the glycolytic pathway does not end up as lactate or go into TCA in B cells stimulated *in vitro*. Instead, pyruvate and other glycolytic intermediates mainly branch into pentose phosphate pathway for DNA and RNA synthesis to support B cell proliferation. Interestingly, glutamine is shown to be oxidized for fueling TCA and enhancing OXPHOS in these activated B cells (Waters et al., 2018). Here, we show that in the quiescent naive B cells, HIF-1α is accumulated when VHL is ablated and glycolysis is enhanced, as evidenced by their enhanced ECAR and elevated lactate level. Similar to the

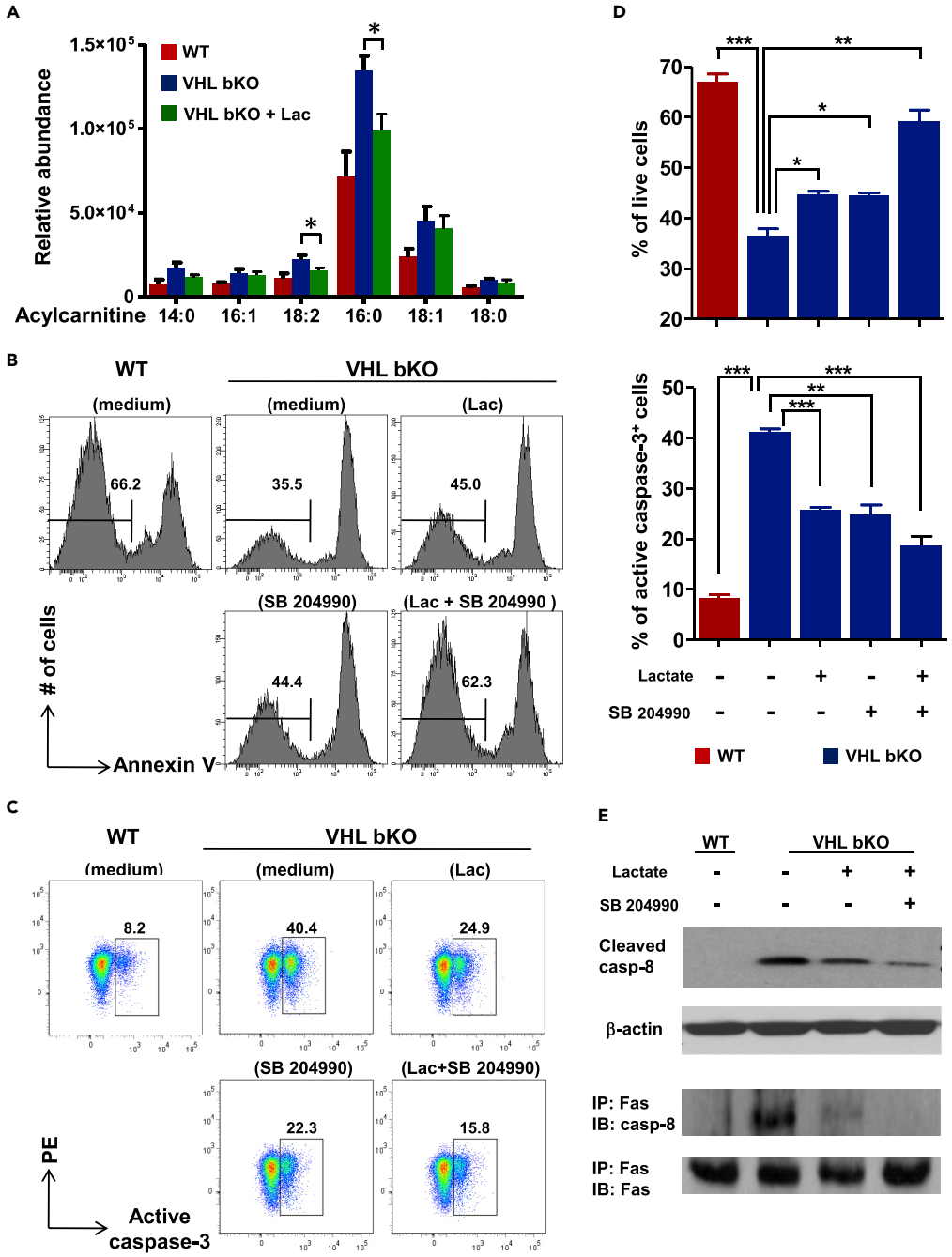

Figure 6. Effect of Lactate Supplementation and ACLY Inhibition on VHL-Deficient B Cells

(A) Abundance of major acylcarnitine species in B cells. WT and VHL-deficient B cells were cultured for 2 h with or without lactate (Lac) (25 mM) as indicated and subjected to lipid metabolite extraction and ultra-performance LC-MS analysis. The relative abundance of acylcarnitine was normalized to total protein in each sample.

(B and C) Flow cytometric analysis of survival and caspase-3 activation of VHL-deficient B cells after lactate supplementation and ACLY inhibition. VHL-deficient B cells were cultured with lactate (25 mM), ACLY inhibitor SB 204990 (50 μM), or both for 6 h. Annexin V^- live cells (B) and cells with active caspase-3 (C) were examined by flow cytometry.

(D) Quantification of live cells and cells with active caspase-3 in different cultures. Percentage of Annexin V^- live (upper panel) and caspase-3^+ (lower panel) cells was quantified based on flow cytometric analysis.

(E) Immunoblotting of caspase-8 activation and DISC formation in VHL-deficient B cells. Whole-cell lysate from VHL-deficient B cells cultured for 2 h under different conditions as indicated was subjected to immunoblotting for the detection of cleaved caspase-8 (upper panel). β-Actin was used as loading control. For the detection of DISC formation,

Figure 6. *Continued*

whole-cell lysate was subjected to immunoprecipitation with anti-Fas antibody followed by the detection of Fas-associated caspase-8 by immunoblotting.

Bar graphs represent mean ± SD (A, n = 3; D, n = 5). Data are representative of 3 (E) or 5 (B and C) experiments. *$p < 0.05$, **$p < 0.01$, ***$p < 0.001$ (Student's t test). See also Figure S6.

stimulated B cells, our metabolomics study reveals that the VHL-deficient quiescent B cells also exhibit higher levels of some metabolites of nucleic acid species, such as adenosine monophosphate, uridine 5′-monophosphate, guanosine monophosphate, guanine, and guanosine (Table S2), suggesting that the carbon source from the enhanced glucose flux through glycolysis also deviates into the pentose phosphate pathway to certain extent. Together with the finding that the reductive glutamine metabolism is abnormally triggered in the VHL-deficient quiescent B cells, which eventually leads to their increased cell death, these results suggest that the fates of quiescent and stimulated B cells are differentially regulated by different metabolic pathways.

The activation of reductive glutamine metabolic pathway in VHL-deficient B cells is reminiscent of the metabolic re-programming in tumor cells under hypoxia or with VHL mutations, where reductive carboxylation of α-KG is also triggered (Metallo et al., 2011; Gameiro et al., 2013). However, the similar metabolic re-programming leads to vastly different outcomes in the two scenarios. In the tumor cells, which have high demands for lipids, reductive carboxylation of α-KG is necessary for *de novo* lipogenesis to support the growth of tumor cells under either *bona fide* or "pseudo" hypoxic conditions (Mullen et al., 2011; Metallo et al., 2011; Wise et al., 2011; Filipp et al., 2012). On the contrary, in the quiescent naive B cells, the activation of reductive carboxylation of α-KG is rather disastrous as it causes constitutive caspase-8 activation and apoptosis. Our data reveal for the first time a link between metabolic imbalance and activation of programmed cell death machinery in naive B cells.

Previous studies showed that VHL deletion in thymocytes caused dramatic reduction in thymic cellularity. The defect was apparently not due to enhanced intrinsic apoptotic pathway and could not be rescued by transgenic expression of Bcl-2 or Bcl-xL or inhibiting caspase-9. Although the activation of caspase-8 was shown to be significantly increased in VHL-deficient thymocytes (Biju et al., 2004), the detailed underlying mechanism remained unresolved. Our data suggest that the enhanced caspase-8 activation in VHL-deficient B cells is not through complexed transcriptional regulation of cell survival genes. Instead, post-translational palmitoylation of death receptor Fas, arising from distorted metabolism, causes enhanced DISC assembly and caspase-8 activation.

Equally fascinating is that pharmacological interference with the metabolic imbalance could reverse the survival defect of VHL-deficient B cells. Lactate supplementation partially reduces ECAR and increases OCR and more importantly, alleviates the increased LCAC levels in VHL-deficient B cells by blocking reductive carboxylation of α-KG. Interestingly, it significantly reduces caspase-8 activation and rescues the impaired survival of VHL-deficient B cells. More strikingly, blockade of reductive carboxylation of α-KG by combinatory lactate supplementation and ACLY inhibition could efficiently inhibit constitutive DISC formation and caspase-8 activation and largely rescue the survival defect of VHL-deficient cells, highlighting the importance of balanced metabolism for naive B cell survival.

In summary, our findings discover a previously unappreciated mechanism by which VHL/HIF-1 pathway metabolically regulates the survival of naive B cells. By balancing glycolytic and oxidative metabolisms, this pathway is able to control carbon entry into TCA cycle and the contribution of reductive glutamine metabolism to lipogenesis, thereby regulating the survival of naive B cells. Our study potentially identifies a pathway that could be metabolically targeted for B cell-driven ailments such as systemic lupus erythematosis.

Limitations of the Study

As VHL also regulates the stability of HIF2α, it cannot be ruled out that the accumulation of HIF2α in VHL-deficient B cells might contribute to the metabolic and survival defects of VHL-mutant B cells to certain extent. More complete studies of B cell-specific HIF1α/HIF2α, HIF2α/VHL DKO, and HIF1α/HIF2α/VHL TKO mice will be important addition to the current study for understanding exactly the role of these molecules in regulating the metabolism and survival of naive B cells. Moreover, it would be interesting to know if other hematopoietic lineages are affected indirectly in VHL-deficient mice.

METHODS

All methods can be found in the accompanying Transparent Methods supplemental file.

SUPPLEMENTAL INFORMATION

Supplemental Information can be found online at https://doi.org/10.1016/j.isci.2019.07.002.

ACKNOWLEDGMENTS

We thank Nicholas Seah for maintenance of mouse colonies and Wee-Lee Lim for help with histology studies. This work was funded by Singapore Agency for Science Technology and Research.

AUTHORS CONTRIBUTIONS

X.S. and L.K.P. designed experiments. X.S., H.J., H.Y., A.M., O.X., C.S., M.S., Y.L.Y., H.Y.S, N.S.W., T.A., and L.A. performed experiments. X.S. and L.K.P. wrote the manuscript. The authors declare no competing financial interests.

DECLARATION OF INTERESTS

The authors declare no competing interests.

Received: November 27, 2018
Revised: March 6, 2019
Accepted: July 1, 2019
Published: July 26, 2019

REFERENCES

Abbott, R.K., Thayer, M., Labuda, J., Silva, M., Philbrook, P., Cain, D.W., Kojima, H., Hatfield, S., Sethumadhavan, S., Ohta, A., et al. (2016). Germinal center hypoxia potentiates immunoglobulin class switch recombination. J. Immunol. *197*, 4014–4020.

Biju, M.P., Neumann, A.K., Bensinger, S.J., Johnson, R.S., Turka, L.A., and Haase, V.H. (2004). Vhlh gene deletion induces Hif-1-mediated cell death in thymocytes. Mol. Cell. Biol. *24*, 9038–9047.

Boothby, M., and Rickert, R.C. (2017). Metabolic regulation of the immune humoral response. Immunity *46*, 743–755.

Caro-Maldonado, A., Wang, R., Nichols, A.G., Kuraoka, M., Milasta, S., Sun, L.D., Gavin, A.L., Abel, E.D., Kelsoe, G., Green, D.R., and Rathmell, J.C. (2014). Metabolic reprogramming is required for antibody production that is suppressed in anergic but exaggerated in chronically BAFF-exposed B cells. J. Immunol. *192*, 3626–3636.

Chakrabandhu, K., Herincs, Z., Huault, S., Dost, B., Peng, L., Conchonaud, F., Marguet, D., He, H.T., and Hueber, A.O. (2007). Palmitoylation is required for efficient Fas cell death signaling. EMBO J. *26*, 209–220.

Chinnadurai, G., Vijayalingam, S., and Gibson, S.B. (2008). BNIP3 subfamily BH3-only proteins: mitochondrial stress sensors in normal and pathological functions. Oncogene *27* (*Suppl 1*), S114–S127.

Cho, S.H., Raybuck, A.L., Stengel, K., Wei, M., Beck, T.C., Volanakis, E., Thomas, J.W., Hiebert, S., Haase, V.H., and Boothby, M.R. (2016). Germinal centre hypoxia and regulation of antibody qualities by a hypoxia response system. Nature *537*, 234–238.

Cramer, T., Yamanishi, Y., Clausen, B.E., Forster, I., Pawlinski, R., Mackman, N., Haase, V.H., Jaenisch, R., Corr, M., Nizet, V., et al. (2003). HIF-1alpha is essential for myeloid cell-mediated inflammation. Cell *112*, 645–657.

Dang, E.V., Barbi, J., Yang, H.Y., Jinasena, D., Yu, H., Zheng, Y., Bordman, Z., Fu, J., Kim, Y., Yen, H.R., et al. (2011). Control of T(H)17/T(reg) balance by hypoxia-inducible factor 1. Cell *146*, 772–784.

Doedens, A.L., Phan, A.T., Stradner, M.H., Fujimoto, J.K., Nguyen, J.V., Yang, E., Johnson, R.S., and Goldrath, A.W. (2013). Hypoxia-inducible factors enhance the effector responses of CD8(+) T cells to persistent antigen. Nat. Immunol. *14*, 1173–1182.

Doughty, C.A., Bleiman, B.F., Wagner, D.J., Dufort, F.J., Mataraza, J.M., Roberts, M.F., and Chiles, T.C. (2006). Antigen receptor-mediated changes in glucose metabolism in B lymphocytes: role of phosphatidylinositol 3-kinase signaling in the glycolytic control of growth. Blood *107*, 4458–4465.

Dufort, F.J., Bleiman, B.F., Gumina, M.R., Blair, D., Wagner, D.J., Roberts, M.F., Abu-Amer, Y., and Chiles, T.C. (2007). Cutting edge: IL-4-mediated protection of primary B lymphocytes from apoptosis via Stat6-dependent regulation of glycolytic metabolism. J. Immunol. *179*, 4953–4957.

Feig, C., Tchikov, V., Schutze, S., and Peter, M.E. (2007). Palmitoylation of CD95 facilitates formation of SDS-stable receptor aggregates that initiate apoptosis signaling. EMBO J. *26*, 221–231.

Fendt, S.M., Bell, E.L., Keibler, M.A., Olenchock, B.A., Mayers, J.R., Wasylenko, T.M., Vokes, N.I., Guarente, L., Vander Heiden, M.G., and Stephanopoulos, G. (2013). Reductive glutamine metabolism is a function of the alpha-ketoglutarate to citrate ratio in cells. Nat. Commun. *4*, 2236.

Filipp, F.V., Scott, D.A., Ronai, Z.A., Osterman, A.L., and Smith, J.W. (2012). Reverse TCA cycle flux through isocitrate dehydrogenases 1 and 2 is required for lipogenesis in hypoxic melanoma cells. Pigment Cell Melanoma Res. *25*, 375–383.

Gallou, C., Joly, D., Mejean, A., Staroz, F., Martin, N., Tarlet, G., Orfanelli, M.T., Bouvier, R., Droz, D., Chretien, Y., et al. (1999). Mutations of the VHL gene in sporadic renal cell carcinoma: definition of a risk factor for VHL patients to develop an RCC. Hum. Mutat. *13*, 464–475.

Gameiro, P.A., Yang, J., Metelo, A.M., Perez-Carro, R., Baker, R., Wang, Z., Arreola, A., Rathmell, W.K., Olumi, A., Lopez-Larrubia, P., et al. (2013). In vivo HIF-mediated reductive carboxylation is regulated by citrate levels and sensitizes VHL-deficient cells to glutamine deprivation. Cell Metab. *17*, 372–385.

Goda, N., Ryan, H.E., Khadivi, B., McNulty, W., Rickert, R.C., and Johnson, R.S. (2003). Hypoxia-inducible factor 1alpha is essential for cell cycle arrest during hypoxia. Mol. Cell. Biol. *23*, 359–369.

Goodnow, C.C., Vinuesa, C.G., Randall, K.L., Mackay, F., and Brink, R. (2010). Control systems and decision making for antibody production. Nat. Immunol. *11*, 681–688.

Gustafsson, A.B. (2011). Bnip3 as a dual regulator of mitochondrial turnover and cell death in the myocardium. Pediatr. Cardiol. *32*, 267–274.

Hamacher-Brady, A., Brady, N.R., Logue, S.E., Sayen, M.R., Jinno, M., Kirshenbaum, L.A., Gottlieb, R.A., and Gustafsson, A.B. (2007). Response to myocardial ischemia/reperfusion injury involves Bnip3 and autophagy. Cell Death Differ. *14*, 146–157.

Hao, Z., Duncan, G.S., Seagal, J., Su, Y.W., Hong, C., Haight, J., Chen, N.J., Elia, A., Wakeham, A., Li, W.Y., et al. (2008). Fas receptor expression in germinal-center B cells is essential for T and B lymphocyte homeostasis. Immunity *29*, 615–627.

Huckabee, W.E. (1956). Control of concentration gradients of pyruvate and lactate across cell membranes in blood. J. Appl. Physiol. *9*, 163–170.

James, G., and Olson, E.N. (1990). Fatty acylated proteins as components of intracellular signaling pathways. Biochemistry *29*, 2623–2634.

Jellusova, J., Cato, M.H., Apgar, J.R., Ramezani-Rad, P., Leung, C.R., Chen, C., Richardson, A.D., Conner, E.M., Benschop, R.J., Woodgett, J.R., and Rickert, R.C. (2017). Gsk3 is a metabolic checkpoint regulator in B cells. Nat. Immunol. *18*, 303–312.

Kim, J.W., Tchernyshyov, I., Semenza, G.L., and Dang, C.V. (2006). HIF-1-mediated expression of pyruvate dehydrogenase kinase: a metabolic switch required for cellular adaptation to hypoxia. Cell Metab. *3*, 177–185.

Kischkel, F.C., Hellbardt, S., Behrmann, I., Germer, M., Pawlita, M., Krammer, P.H., and Peter, M.E. (1995). Cytotoxicity-dependent APO-1 (Fas/CD95)-associated proteins form a death-inducing signaling complex (DISC) with the receptor. EMBO J. *14*, 5579–5588.

Kojima, H., Gu, H., Nomura, S., Caldwell, C.C., Kobata, T., Carmeliet, P., Semenza, G.L., and Sitkovsky, M.V. (2002). Abnormal B lymphocyte development and autoimmunity in hypoxia-inducible factor 1alpha -deficient chimeric mice. Proc. Natl. Acad. Sci. U S A *99*, 2170–2174.

Lee, J.H., Elly, C., Park, Y., and Liu, Y.C. (2015). E3 ubiquitin ligase VHL regulates hypoxia-inducible factor-1alpha to maintain regulatory T cell stability and suppressive capacity. Immunity *42*, 1062–1074.

Lemm, I., Lingott, A., Strandmann, E., Zoidl, C., Bulman, M.P., Hattersley, A.T., Schulz, W.A., Ebert, T., and Ryffel, G.U. (1999). Loss of HNF1alpha function in human renal cell carcinoma: frequent mutations in the VHL gene but not the HNF1alpha gene. Mol. Carcinog. *24*, 305–314.

Metallo, C.M., Gameiro, P.A., Bell, E.L., Mattaini, K.R., Yang, J., Hiller, K., Jewell, C.M., Johnson, Z.R., Irvine, D.J., Guarente, L., et al. (2011). Reductive glutamine metabolism by IDH1 mediates lipogenesis under hypoxia. Nature *481*, 380–384.

Mintun, M.A., Vlassenko, A.G., Rundle, M.M., and Raichle, M.E. (2004). Increased lactate/pyruvate ratio augments blood flow in physiologically activated human brain. Proc. Natl. Acad. Sci. U S A *101*, 659–664.

Mullen, A.R., Wheaton, W.W., Jin, E.S., Chen, P.H., Sullivan, L.B., Cheng, T., Yang, Y., Linehan, W.M., Chandel, N.S., and DeBerardinis, R.J. (2011). Reductive carboxylation supports growth in tumour cells with defective mitochondria. Nature *481*, 385–388.

Nadolski, M.J., and Linder, M.E. (2007). Protein lipidation. FEBS J. *274*, 5202–5210.

O'Sullivan, T.E., Johnson, L.R., Kang, H.H., and Sun, J.C. (2015). BNIP3- and BNIP3L-mediated mitophagy promotes the generation of natural killer cell memory. Immunity *43*, 331–342.

Olenchock, B.A., Rathmell, J.C., and Vander Heiden, M.G. (2017). Biochemicphenotypesal underpinnings of immune cell metabolic. Immunity *46*, 703–713.

Palazon, A., Goldrath, A.W., Nizet, V., and Johnson, R.S. (2014). HIF transcription factors, inflammation, and immunity. Immunity *41*, 518–528.

Rajewsky, K. (1996). Clonal selection and learning in the antibody system. Nature *381*, 751–758.

Resh, M.D. (2012). Targeting protein lipidation in disease. Trends Mol. Med. *18*, 206–214.

Salaun, C., Greaves, J., and Chamberlain, L.H. (2010). The intracellular dynamic of protein palmitoylation. J. Cell Biol. *191*, 1229–1238.

Schmidt-Kastner, R., Aguirre-Chen, C., Kietzmann, T., Saul, I., Busto, R., and Ginsberg, M.D. (2004). Nuclear localization of the hypoxia-regulated pro-apoptotic protein BNIP3 after global brain ischemia in the rat hippocampus. Brain Res. *1001*, 133–142.

Semenza, G.L. (2001). HIF-1, O(2), and the 3 PHDs: how animal cells signal hypoxia to the nucleus. Cell *107*, 1–3.

Shi, L.Z., Wang, R., Huang, G., Vogel, P., Neale, G., Green, D.R., and Chi, H. (2011). HIF1alpha-dependent glycolytic pathway orchestrates a metabolic checkpoint for the differentiation of TH17 and Treg cells. J. Exp. Med. *208*, 1367–1376.

Wang, R., Dillon, C.P., Shi, L.Z., Milasta, S., Carter, R., Finkelstein, D., McCormick, L.L., Fitzgerald, P., Chi, H., Munger, J., and Green, D.R. (2011). The transcription factor Myc controls metabolic reprogramming upon T lymphocyte activation. Immunity *35*, 871–882.

Waters, L.R., Ahsan, F.M., Wolf, D.M., Shirihai, O., and Teitell, M.A. (2018). Initial B cell activation induces metabolic reprogramming and mitochondrial remodeling. iScience *5*, 99–109.

Wise, D.R., Ward, P.S., Shay, J.E., Cross, J.R., Gruber, J.J., Sachdeva, U.M., Platt, J.M., DeMatteo, R.G., Simon, M.C., and Thompson, C.B. (2011). Hypoxia promotes isocitrate dehydrogenase-dependent carboxylation of alpha-ketoglutarate to citrate to support cell growth and viability. Proc. Natl. Acad. Sci. U S A *108*, 19611–19616.

ISCI, Volume *17*

Supplemental Information

von Hippel-Lindau Protein Maintains Metabolic Balance to Regulate the Survival of Naive B Lymphocytes

Shengli Xu, Jianxin Huo, Yuhan Huang, Melissa Aw, Shuwen Chen, Shiya Mak, Lian Yee Yip, Ying Swan Ho, Sze Wai Ng, Andy Hee-Meng Tan, Alison Lee, Xijun Ou, and Kong-Peng Lam

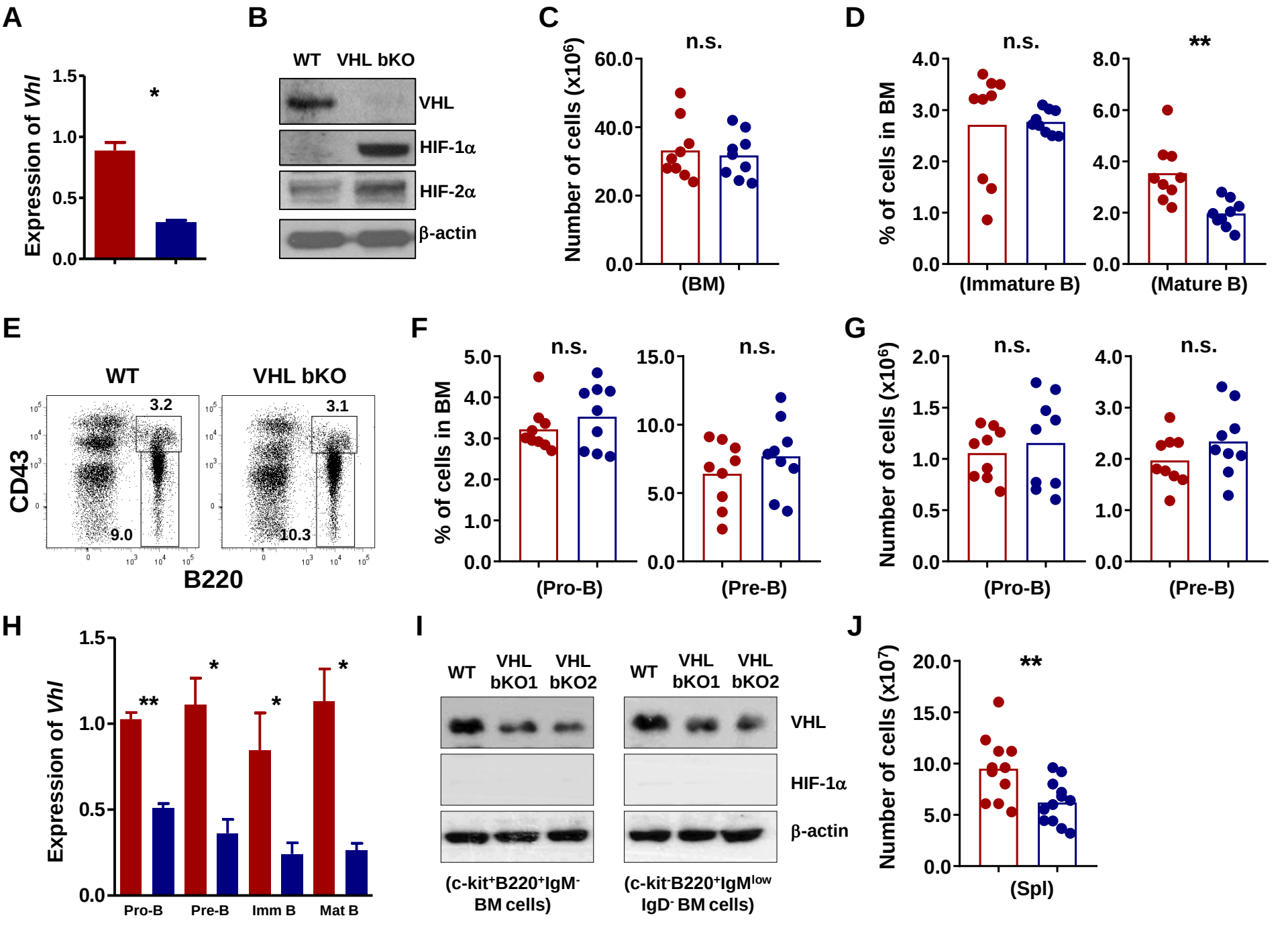
A
Expression of Vhl
1.5
1.0
0.5
0.0
*
B
WT
VHL bKO
VHL
HIF-1α
HIF-2α
β-actin
C
n.s.
Number of cells (x10⁶)
60.0
40.0
20.0
0.0
(BM)
D
n.s.
**
% of cells in BM
4.0
3.0
2.0
1.0
0.0
8.0
6.0
4.0
2.0
0.0
(Immature B)
(Mature B)
E
WT
VHL bKO
3.2
3.1
9.0
10.3
CD43
B220
F
n.s.
n.s.
% of cells in BM
5.0
4.0
3.0
2.0
1.0
0.0
15.0
10.0
5.0
0.0
(Pro-B)
(Pre-B)
G
n.s.
n.s.
Number of cells (x10⁶)
2.0
1.5
1.0
0.5
0.0
4.0
3.0
2.0
1.0
0.0
(Pro-B)
(Pre-B)
H
Expression of Vhl
1.5
1.0
0.5
0.0
**
*
*
*
Pro-B
Pre-B
Imm B
Mat B
I
WT
VHL bKO1
VHL bKO2
WT
VHL bKO1
VHL bKO2
VHL
HIF-1α
β-actin
(c-kit⁺B220⁺IgM⁻ BM cells)
(c-kit⁻B220⁺IgM^low IgD⁻ BM cells)
J
**
Number of cells (x10⁷)
20.0
15.0
10.0
5.0
0.0
(Spl)

Figure S1. Deletion of VHL and accumulation of HIF in VHL bKO B cells, Related to Figure 1. (**A**, **H**) Gene expression of *Vhl* in VHL bKO B cells. Total B (IgM^+B220^+) cells from spleen (**A**) and pro-B ($IgM^-IgD^-B220^+CD43^+$), pre-B ($IgM^-IgD^-B220^+CD43^-$), immature ($B220^+IgM^+IgD^-$) and mature ($B220^+IgM^+IgD^+$) B cells from BM (**H**) were sorted from WT and VHL bKO mice. *Vhl* mRNA level was examined by qRT-PCR. Gene expression of *Vhl* in VHL bKO B cells (blue) was presented relative to that in WT B cells (red), set as 1. Bar graphs represent mean ± SD (n=3). (**B**, **I**) Immunoblotting of VHL, HIF proteins in WT and VHL bKO B cells. Protein levels of VHL, HIF-1α and HIF-2α in total splenic (IgM^+B220^+) (**B**), BM pro-B/pre-B ($IgM^-IgD^-B220^+$) and immature ($B220^+IgM^+IgD^-$) (**I**) B cells from WT and VHL bKO mice were examined with specific antibodies. β-actin was included as loading control. Data shown are representative of 3 experiments. (**C**, **D**, **F**, **G** and **J**) Percentage and absolute number of various cell populations in the BM and spleens of WT and VHL bKO mice. The absolute number of total BM cells (**C**), pro-B ($IgM^-IgD^-B220^+CD43^+$) (**G**, left), pre-B ($IgM^-IgD^-B220^+CD43^-$) (**G**, right) in the BM, total splenocytes (**J**) and the percentage of immature B ($B220^+IgM^+IgD^-$) (**D**, left), mature B ($B220^+IgM^+IgD^+$) (**D** right), pro-B ($IgM^-IgD^-B220^+CD43^+$) (**F**, left), pre-B ($IgM^-IgD^-B220^+CD43^-$) (**F**, right) cells in the BM of WT (red) and VHL bKO (blue) mice were calculated based on total cell count and their percentage as determined by flow cytometry. (**E**) Flow cytometric analysis of early B cell populations in the BM of WT and VHL bKO mice. Numbers adjacent to outline areas indicate the percentage of gated pro-B ($IgM^-IgD^-B220^+CD43^+$) and pre-B ($IgM^-IgD^-B220^+CD43^-$) cells over total BM cells. Data shown are representative of more than 5 independent experiments. n.s., not significant, *, $p<0.05$; *, $p<0.01$. For the enumeration of BM cells, cells were obtained from one femur and tibia of mice that were 8-12 weeks old.

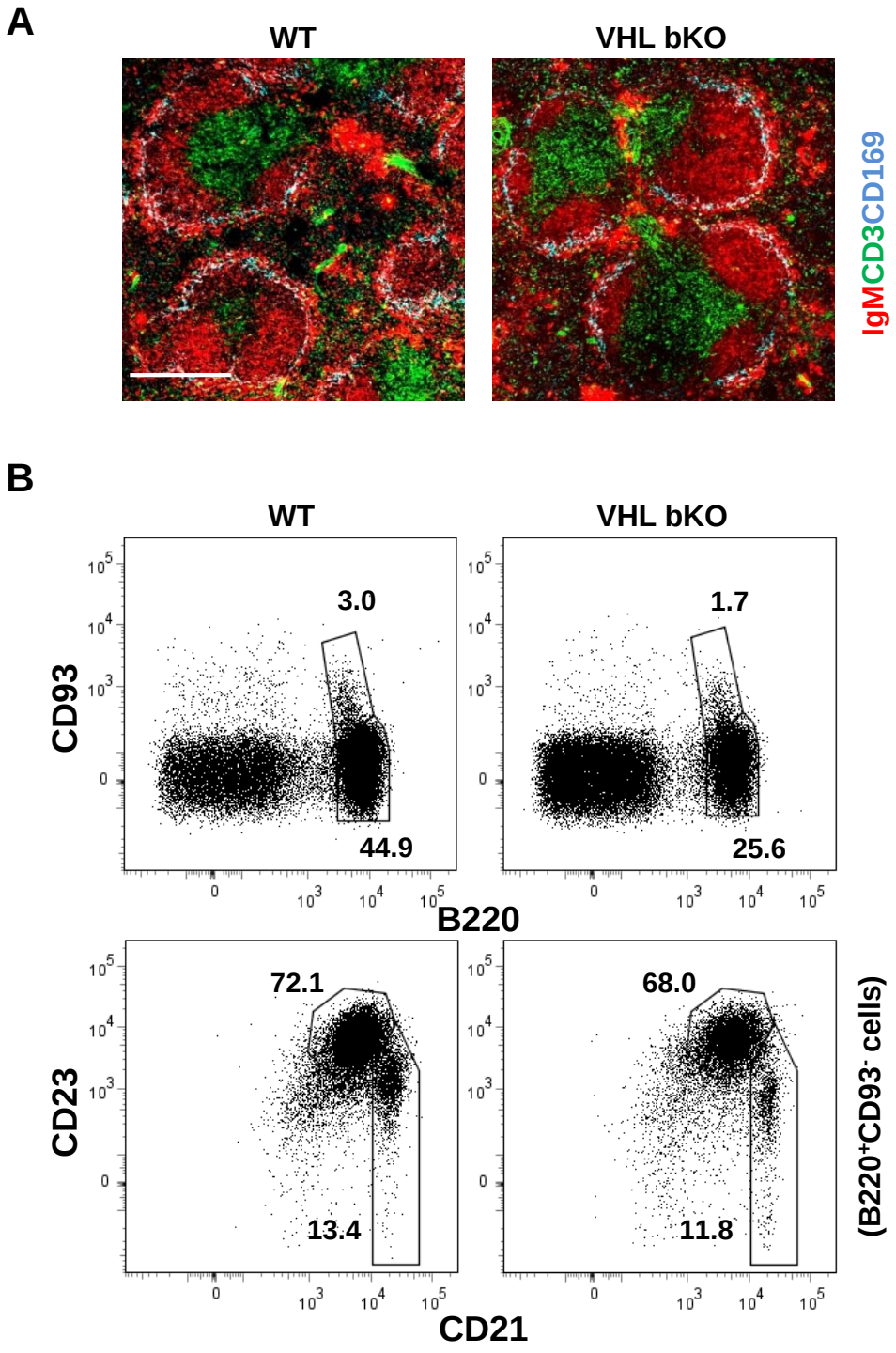

Figure S2. Analysis of splenic marginal zone B cells in VHL bKO mice, Related to Figure 2.
(**A**) Microscopy of spleen sections of WT and VHL bKO mice. B cells (red), T cells (green) and marginal metallophilic macrophages (blue) were stained with anti-IgM, anti-CD3 and anti-CD169 antibodies, respectively. Scale bar: 100 μm. (**B**) Flow cytometric analysis of marginal zone B cells in spleens of WT and VHL bKO mice. Numbers adjacent to outline areas indicate the percentage of total splenocytes (upper panel) or mature B ($B220^{+}CD93^{-}$) cells (lower panel). Data shown are representative of 3 (**A**) or 8 (**B**) independent experiments.

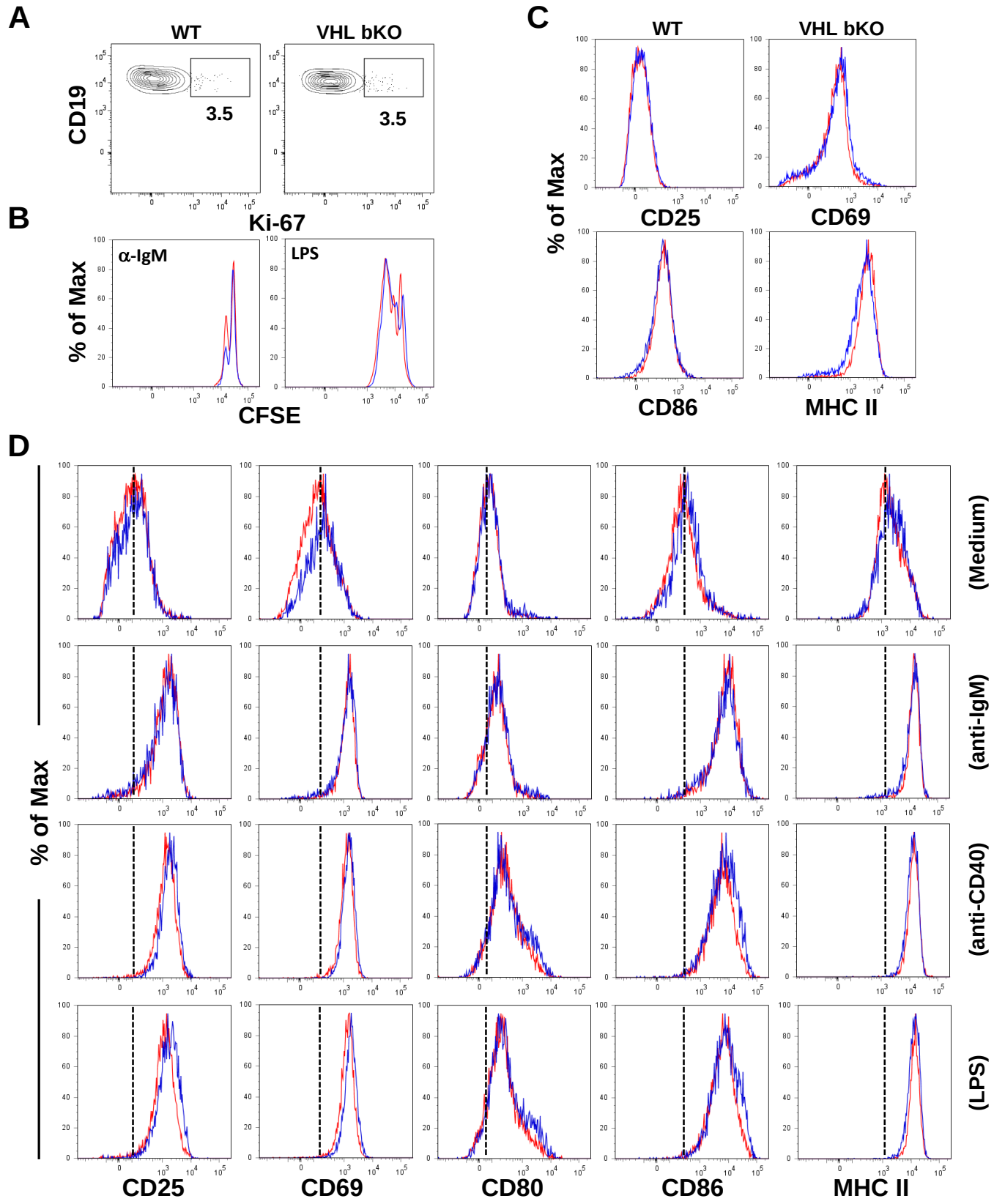

Figure S3. Normal upregulation of activation markers of VHL bKO B cells upon stimulation, Related Figure 3. (**A, B**) Flow cytometric analysis of B cell proliferation. Proliferation of WT and VHL bKO splenic B cells was examined *ex vivo* by flow cytometry for Ki-67 expression (**A**). *In vitro* proliferation of WT (red) and VHL bKO

(blue) B cells were determined by flow cytometry of CFSE-labelled cells after treatment with anti-IgM antibody (20 μg/ml) or LPS (1 μg/ml) for 3 days (**B**). (**C, D**) Flow cytometric analysis of B cell activation. Cell surface expression of various activation markers on *ex vivo* B cells (**C**) or cells unstimulated or stimulated with anti-IgM (20 μg/ml) or anti-CD40 (1 μg/ml) antibodies or LPS (100 ng/ml) for 16 hr (**D**). Data shown are representative of 5 (**A**-**C**) or 3 (**D**) independent experiments.

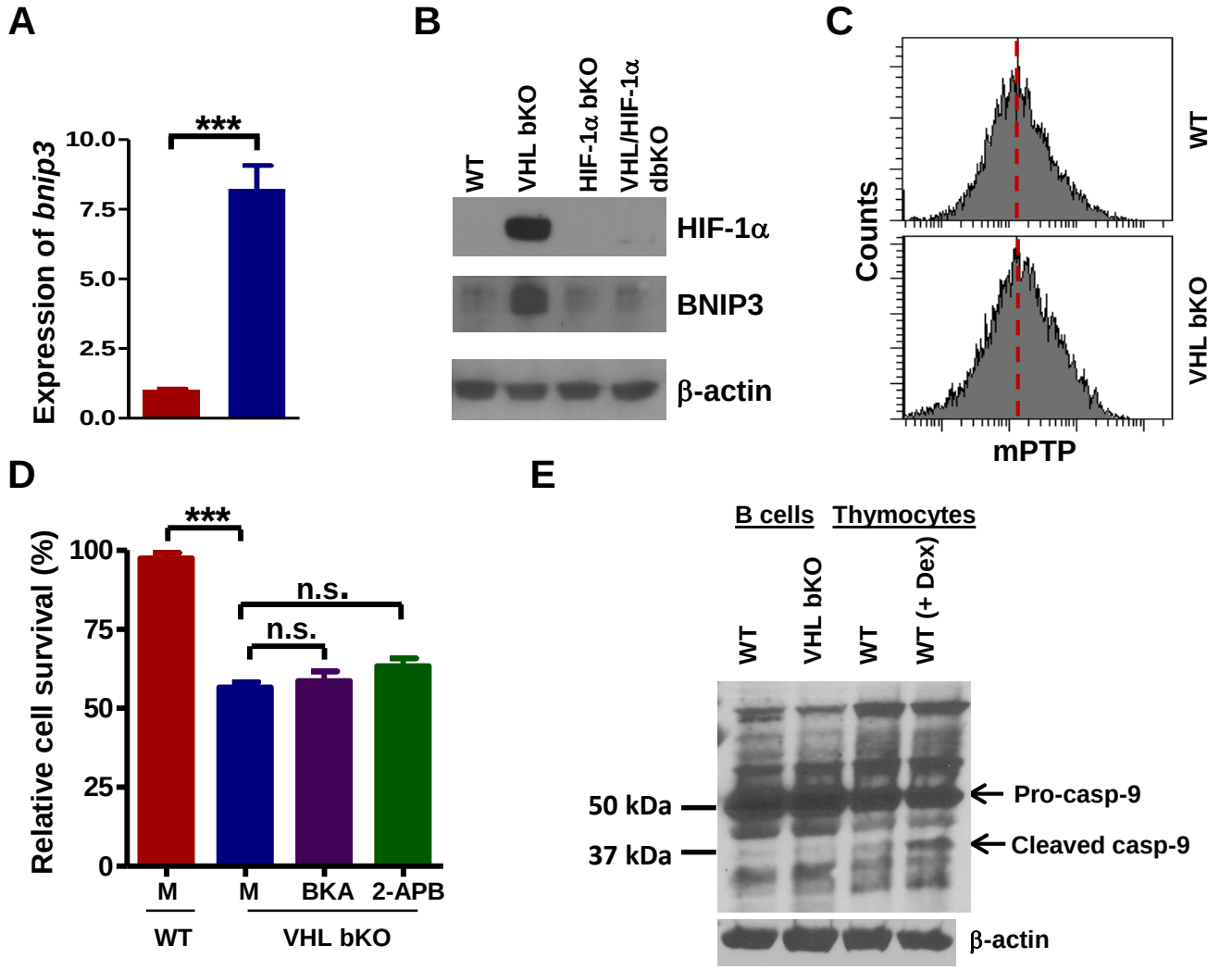

Figure S4. Upregulation BNIP3 in VHL bKO B cells, Related to Figure 4. (**A**) Elevated mRNA levels of *bnip3* in VHL bKO cells. *Bnip3* mRNA level in VHL bKO B cells (blue bar) was examined by qRT-PCR and presented relative to that in WT B cells (red bar), set as 1. (**B**) Increased protein level of BNIP3 in VHL bKO B cells. HIF-1α and BNIP3 protein levels in B cells of various genotypes were examined by immunoblotting with specific antibodies. (**C**) Flow cytometry of mitochondrial permeability transition pore (mPTP) opening in quiescent B cells. Splenic VHL bKO and control B cells were labelled with mPTP staining dye and analysed by flow cytometry. (**D**) Survival of VHL bKO B cells with or without treatment of BKA and 2-APB. The survival of VHL bKO B cells under various culture conditions was presented relative to that of WT B cells, set as 100%. (**E**) Caspase-9 activation status in VHL bKO B cells. Pro- and cleaved-caspase-9 in WT and VHL bKO B cells were examined by immunoblotting. Thymocytes from WT mice treated with dexamethasone (+ Dex) were served as positive controls for caspase-9 activation. β-actin was used as loading control. Bar graphs represent mean ± SD (n=3). Data shown are representative of 3 (**A**, **C**, **D** and **E**) or 2 (**B**) independent experiments. n.s. not significant; ***, $p<0.001$.

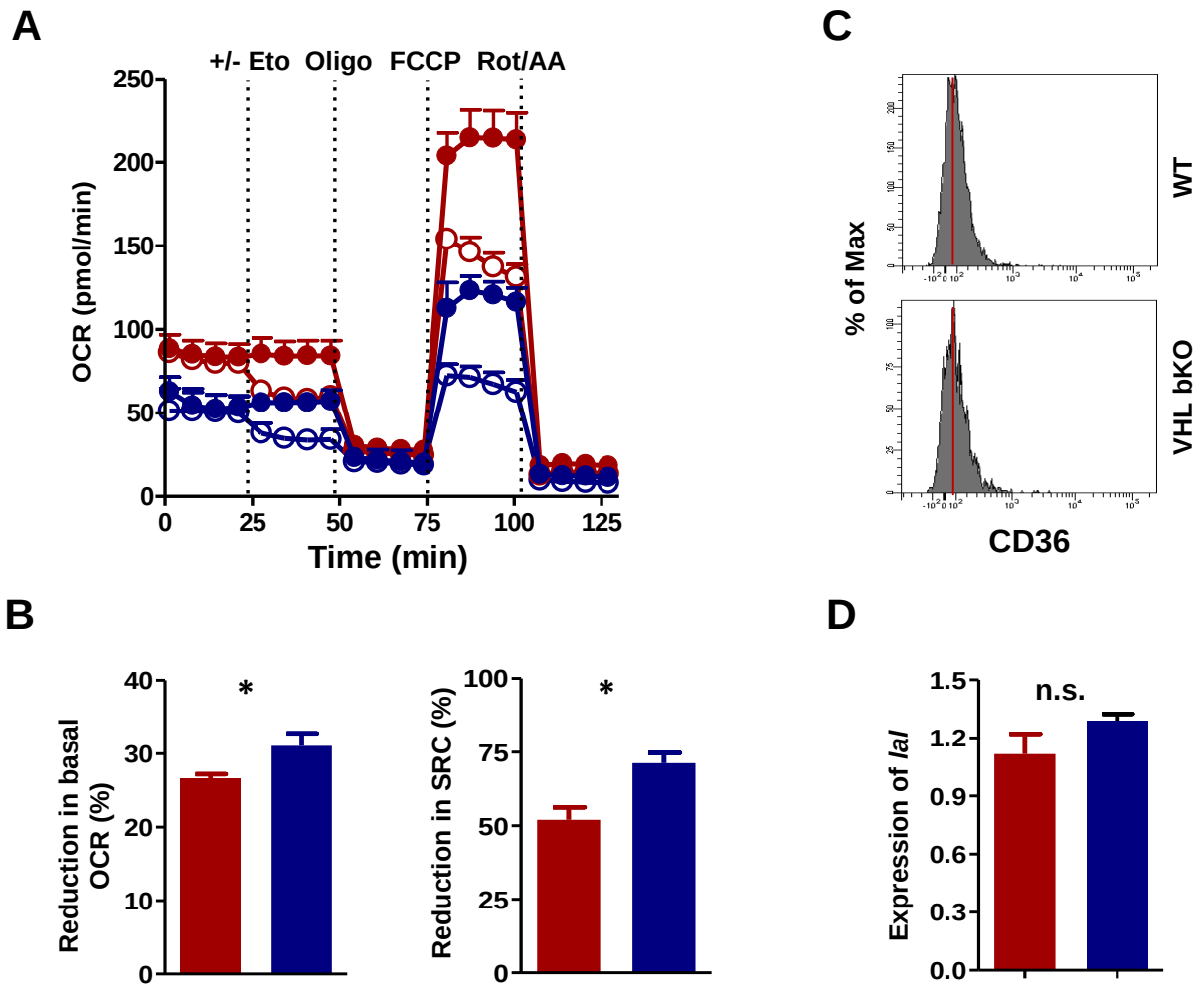

Figure S5. Normal FAO and CD36 and LAL expression in VHL bKO B cells, Related to Figure 5. (**A**) OCR in B cells with or without treatment of Etomoxir (Eto). OCR of WT (red) and VHL bKO (blue) B cells with (open circles) or without (filled circles) Eto (200 μM) treatment was measured in real-time. Oligomycin (Oligo) (1.0 μM), mitochondrial uncoupler FCCP (1.0 μM) and electron transport inhibitors rotenone plus antimycin (Rot/AA) (0.5 μM for each) were added as indicated. (**B**) Reduction in basal OCR (left panel) and SRC (right panel) by Etomoxir treatment. Percentage of reduction = (OCR Value$_{-Eto}$ – OCR Value$_{+Eto}$)/ OCR Value$_{-Eto}$. Bar graphs represent mean ± SD (n=4). (**C**) Histogram of flow cytometric analysis of CD36 expression on WT and VHL bKO. (**D**) mRNA level of lysosomal acid lipase (LAL) in WT (red) and VHL bKO (blue) B cells. *Lal* mRNA was examined by qRT-PCR and the gene expression of *lal* in VHL bKO cells was presented relative to that in WT B cells, set as 1. Bar graphs represent mean ± SD (B, n=4; D, n=3). Data shown are representative of 4 (**A**) or 3 (**C**) experiments. n.s., not significant, *, p<0.05.

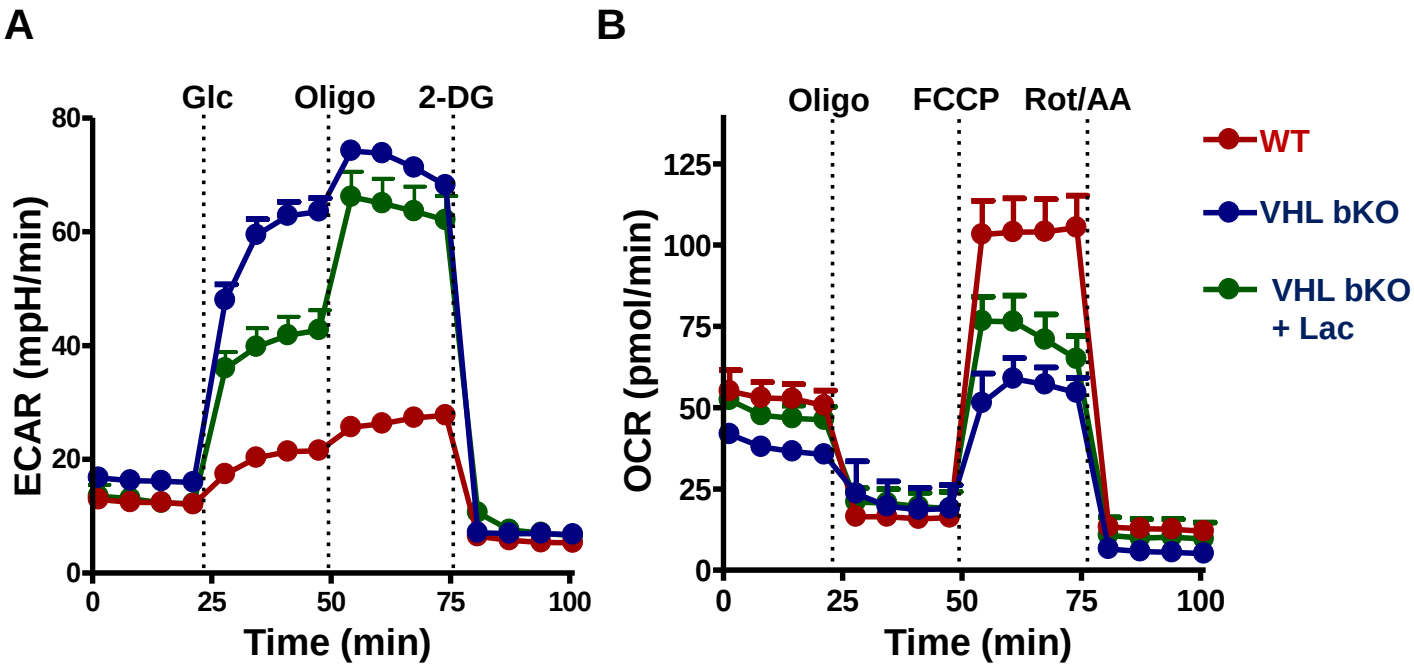

Figure S6. Correction of glycolytic and oxidative metabolic imbalance in VHL bKO B cells by lactate, Related to Figure 6. (**A, B**) Analysis of EACR (**A**) and OCR (**B**) in WT (red), VHL bKO (blue) and VHL bKO B cells treated with lactate (green). For the lactate treatment, VHL bKO B cells were pre-cultured in complete RPMI1640 medium supplemented with lactate (25 μM) for 2 hr before the metabolic analysis. Real-time changes in EACR of B cells was measured with the addition of glucose (Glc) (10 μM), oligomycin (Oligo) (1.0 μM) and 2-Deoxy-D-glucose (2-DG) (50 μM). OCR of B cells was measured in real-time with the addition of oligomycin (Oligo) (1.0 μM), mitochondrial uncoupler FCCP (1.0 μM) and electron transport inhibitors rotenone plus antimycin (Rot/AA) (0.5 μM for each). Data shown are representative of 4 independent experiments.

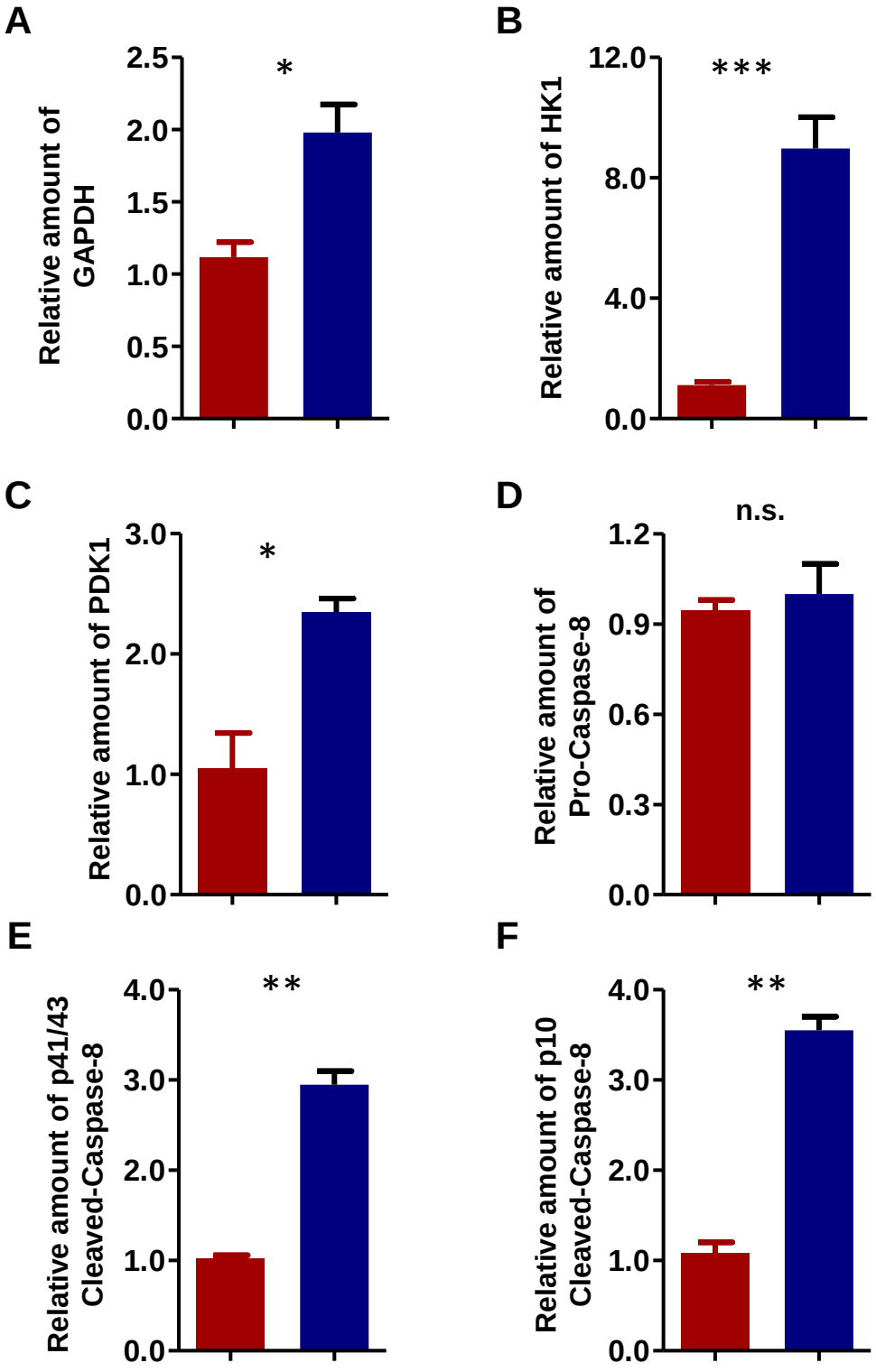

Figure S7. Quantification of protein levels in Immunoblots, Related to Figure 2, 4 and 5. Expression levels of GAPDH (A), HK1 (**B**), PDK1 (**C**), pro-Caspase-8 (**D**), p41/p43 cleaved- (**E**) and p10 cleaved-Caspase 8 (**F**) in WT and VHL bKO B cells as examined by immunoblotting in Figure 2, 4 and 5 were analysed by Image J. Protein levels of various enzymes in VHL bKO B cells (blue) were presented relative to that in WT B cells (red), set as 1. Bar graphs represent mean ± SD (n=3). n.s., not significant; *, $p<0.05$; **, $p<0.01$; ***, $p<0.001$.

Table S1. Differentially Expressed Genes between WT and VHL bKO B cells, Related to Figure 2

Gene name	Gene description	Fold change (KO vs. WT)	*p* -value
Ak4	adenylate kinase 4	29.89	2.08E-03
Mgarp	mitochondria localized glutamic acid rich protein	24.63	1.37E-03
Vldlr	very low density lipoprotein receptor	16.02	4.62E-03
Aldoc	aldolase C, fructose-bisphosphate	13.83	2.24E-03
Rgs11	regulator of G-protein signaling 11	13.44	6.98E-04
Pygl	liver glycogen phosphorylase	12.67	2.54E-03
Bnip3	BCL2/adenovirus E1B interacting protein 3	12.60	1.04E-03
Prelid2	PRELI domain containing 2	7.73	2.94E-03
Tpi1	triosephosphate isomerase 1	7.15	2.16E-03
P4ha1	procollagen-proline, 2-oxoglutarate 4-dioxygenase (proline 4-hydroxylase), alpha 1 poly	6.50	2.96E-03
Sh3d19	SH3 domain protein D19	5.67	8.34E-03
Slc16a3	solute carrier family 16 (monocarboxylic acid transporters), member 3	5.36	9.03E-03
D4Ertd298e	DNA segment, Chr 4, ERATO Doi 298, expressed	5.27	4.01E-03
Hk2	hexokinase 2	5.11	4.49E-03
Pfkl	phosphofructokinase, liver, B-type	4.99	5.65E-03
Mxi1	Max interacting protein 1	4.51	4.40E-03
Pgk1	phosphoglycerate kinase 1	4.48	2.49E-03
Efna1	ephrin A1	4.03	4.18E-03
Sspn	sarcospan	4.01	1.69E-02
Ankrd37	ankyrin repeat domain 37	3.99	6.09E-03
Pfkp	phosphofructokinase, platelet	3.97	2.29E-03
Tnfsf9	tumor necrosis factor (ligand) superfamily, member 9	3.87	4.84E-03
Egln3	EGL nine homolog 3 (C. elegans)	3.86	1.51E-02
Egln1	EGL nine homolog 1 (C. elegans)	3.71	4.25E-03
Pdxp	pyridoxal (pyridoxine, vitamin B6) phosphatase	3.57	1.43E-02
2310068C19Rik	RIKEN cDNA 2310068C19 gene	3.44	5.01E-03
Bnip3l	BCL2/adenovirus E1B interacting protein 3-like /// predicted gene 10480 /// BCL2/adenov	3.37	7.11E-03
Pgm2	phosphoglucomutase 2	3.34	4.87E-03
Ppp1r3b	protein phosphatase 1, regulatory (inhibitor) subunit 3B	3.31	1.40E-02
Gm129	predicted gene 129	3.29	8.98E-03
Plod2	procollagen lysine, 2-oxoglutarate 5-dioxygenase 2	3.27	1.33E-02
Galk1	galactokinase 1	3.23	5.06E-03
Pkm	pyruvate kinase, muscle	3.08	6.32E-03
Kdm5b	lysine (K)-specific demethylase 5B	3.08	9.45E-03
Errfi1	ERBB receptor feedback inhibitor 1	2.99	9.70E-03
Pfkfb3	6-phosphofructo-2-kinase/fructose-2,6-biphosphatase 3	2.94	1.64E-02
Maff	v-maf musculoaponeurotic fibrosarcoma oncogene family, protein F (avian)	2.91	9.22E-03
Car2	carbonic anhydrase 2	2.82	2.10E-03
Eps8l1	EPS8-like 1	2.82	2.15E-02
Cxcr7	chemokine (C-X-C motif) receptor 7	2.81	7.11E-03
BC062258	cDNA sequence BC062258	2.79	1.38E-02
Grhpr	glyoxylate reductase/hydroxypyruvate reductase	2.78	1.29E-02
Pgam1	phosphoglycerate mutase 1	2.75	9.27E-03
Slc2a1	solute carrier family 2 (facilitated glucose transporter), member 1	2.73	9.41E-03
Sap30	sin3 associated polypeptide	2.71	7.22E-03
Ero1l	ERO1-like (S. cerevisiae)	2.70	6.66E-03
Hilpda	hypoxia inducible lipid droplet associated	2.66	2.51E-02
Hpse	heparanase	2.61	2.09E-03
Gm11110	predicted gene 11110	2.57	1.60E-02
Ldha	lactate dehydrogenase A	2.56	5.71E-03
Mif	macrophage migration inhibitory factor	2.55	5.88E-03
Syce2	synaptonemal complex central element protein 2	2.53	2.17E-02
Clybl	citrate lyase beta like	2.53	2.14E-03
Aldoa	aldolase A, fructose-bisphosphate	2.52	5.08E-03
5330426P16Rik	RIKEN cDNA 5330426P16 gene	2.46	8.17E-03
3110057O12Rik	RIKEN cDNA 3110057O12 gene	2.39	1.62E-02
Vegfa	vascular endothelial growth factor A	2.38	4.27E-02
Adm	adrenomedullin	2.34	4.99E-02
Pdk1	pyruvate dehydrogenase kinase, isoenzyme 1	2.31	5.89E-03
2310022B05Rik	RIKEN cDNA 2310022B05 gene	2.29	3.16E-02
Eno1	enolase 1, alpha non-neuron	2.29	6.89E-03
Higd1a	HIG1 domain family, member 1A	2.27	1.16E-02
Fam162a	family with sequence similarity 162, member A	2.23	2.04E-02
Kdm6b	KDM1 lysine (K)-specific demethylase 6B	2.20	2.60E-02
Kcnq5	potassium voltage-gated channel, subfamily Q, member 5	2.20	3.61E-03
Eno1	enolase 1, alpha non-neuron /// predicted gene 5506 /// alpha-enolase-like	2.19	6.59E-03
Anxa4	annexin A4	2.17	5.82E-03
Ndrg1	N-myc downstream regulated gene 1	2.15	2.49E-02
C80012	expressed sequence C80012	2.12	9.70E-03
Lxn	latexin	2.11	2.23E-02
Csrp2	cysteine and glycine-rich protein 2	2.07	4.12E-02
Trim32	tripartite motif-containing 32	2.03	2.15E-02
Kdm3a	lysine (K)-specific demethylase 3A	2.03	4.20E-03
Gapdh	glyceraldehyde-3-phosphate dehydrogenase	2.01	5.01E-03
Trappc6a	trafficking protein particle complex 6A	2.01	1.14E-02
Cd93	CD93 antigen	1.98	2.14E-02
Myb	myeloblastosis oncogene	1.96	4.47E-02
Jmjd6	jumonji domain containing 6	1.95	7.04E-03
Gad1	glutamate decarboxylase 1	1.94	3.48E-02
3000002C10Rik /// Gapdh	glyceraldehyde-3-phosphate dehydrogenase pseudogene /// glyceraldehyde-3-phosphate dehy	1.94	4.63E-03

Slc2a3	solute carrier family 2 (facilitated glucose transporter), member 3	1.93	2.41E-02
Atp8b4	ATPase, class I, type 8B, member 4	1.90	3.00E-02
Lef1	lymphoid enhancer binding factor 1	1.90	1.61E-02
Tmem26	transmembrane protein 26	1.87	1.45E-02
Npepps	aminopeptidase puromycin sensitive	1.86	3.12E-02
Alkbh5	alkB, alkylation repair homolog 5 (E. coli)	1.85	2.53E-02
Gpi1	glucose phosphate isomerase 1	1.85	8.09E-03
Cyp3a11	cytochrome P450, family 3, subfamily a, polypeptide 11 /// PRELI domain-containing prot	1.85	8.53E-03
Plbd1	phospholipase B domain containing 1	1.82	4.13E-02
Kdm4b	lysine (K)-specific demethylase 4B	1.82	9.30E-03
Cfp	complement factor properdin	1.81	2.64E-02
Tube1	epsilon-tubulin 1	1.81	2.48E-03
Gm2011	RIKEN cDNA 3110057O12 gene /// predicted gene 2011	1.80	6.28E-03
Pafah1b3	platelet-activating factor acetylhydrolase, isoform 1b, subunit 3	1.80	1.06E-02
Cpt1a	carnitine palmitoyltransferase 1a, liver	1.79	1.71E-02
Mical3	microtubule associated monooxygenase, calponin and LIM domain containing 3	1.76	1.15E-02
Nedd4	neural precursor cell expressed, developmentally down-regulated 4	1.76	6.06E-03
Heatr2	HEAT repeat containing 2	1.73	1.07E-02
Rlf	rearranged L-myc fusion sequence	1.73	1.57E-02
Pla2g12a	phospholipase A2, group XIIA	1.72	1.88E-02
Agpat5	1-acylglycerol-3-phosphate O-acyltransferase 5 (lysophosphatidic acid acyltransferase,	1.71	2.05E-02
Arhgap31	Rho GTPase activating protein 31	1.70	3.22E-02
Zfp654	zinc finger protein 654	1.70	4.21E-02
Gm14446	predicted gene 14446	1.70	7.04E-03
Rhbdf1	rhomboid family 1 (Drosophila)	1.70	3.78E-02
Acss2	acyl-CoA synthetase short-chain family member 2	1.70	2.64E-02
Asb2	ankyrin repeat and SOCS box-containing 2	1.68	1.40E-02
Mthfd1l	methylenetetrahydrofolate dehydrogenase (NADP+ dependent) 1-like	1.67	2.96E-02
Apba3	amyloid beta (A4) precursor protein-binding, family A, member 3	1.67	1.04E-02
Lgals3	lectin, galactose binding, soluble 3	1.66	1.93E-03
Smpdl3a	sphingomyelin phosphodiesterase, acid-like 3A	1.65	1.17E-03
Prdx4	peroxiredoxin 4	1.65	7.59E-03
Agl	amylo-1,6-glucosidase, 4-alpha-glucanotransferase	1.65	4.49E-02
Hs6st1	heparan sulfate 6-O-sulfotransferase 1	1.64	9.84E-03
Ccdc115	coiled-coil domain containing 115	1.64	1.65E-02
Pfn2	profilin 2	1.64	3.87E-02
Slc30a9	solute carrier family 30 (zinc transporter), member 9	1.63	1.51E-02
Narf	nuclear prelamin A recognition factor	1.62	2.01E-02
Itfg2	integrin alpha FG-GAP repeat containing 2	1.62	4.58E-02
Prelid1	PRELI domain containing 1	1.62	3.03E-03
Whamm	WAS protein homolog associated with actin, golgi membranes and microtubules	1.61	2.37E-02
Gbe1	glucan (1,4-alpha-), branching enzyme 1	1.59	1.34E-02
Agpat9	1-acylglycerol-3-phosphate O-acyltransferase 9	1.59	3.80E-02
Hk1	hexokinase 1	1.59	3.81E-02
Bsg	basigin	1.58	3.42E-02
LOC100046650 /// Prelid1	PRELI domain-containing protein 1, mitochondrial-like /// PRELI domain containing 1	1.57	2.15E-02
Slc37a4	solute carrier family 37 (glucose-6-phosphate transporter), member 4	1.57	2.53E-02
Eif4ebp1	eukaryotic translation initiation factor 4E binding protein 1	1.57	8.22E-03
1200015M12Rik	RIKEN cDNA 1200015M12 gene /// RIKEN cDNA A130040M12 gene	1.57	4.48E-02
Mctp2	multiple C2 domains, transmembrane 2	1.56	2.07E-02
1200003I10Rik	RIKEN cDNA 1200003I10 gene /// RIKEN cDNA 1200015M12 gene /// RIKEN cDNA A130040M12 gen	1.56	2.55E-02
Zfp292	zinc finger protein 292	1.55	3.93E-02
Ogfrl1	opioid growth factor receptor-like 1	1.54	3.07E-02
Slc25a20	solute carrier family 25 (mitochondrial carnitine/acylcarnitine translocase), member 20	1.54	1.95E-02
Fam3a	family with sequence similarity 3, member A	1.54	8.68E-03
Tnfaip3	tumor necrosis factor, alpha-induced protein 3	1.53	1.18E-02
Ripk3	receptor-interacting serine-threonine kinase 3	1.53	3.60E-02
Cryz	crystallin, zeta	1.51	1.44E-02
Ccng2	cyclin G2	1.50	5.67E-03
Sema7a	sema domain, immunoglobulin domain (Ig), and GPI membrane anchor, (semaphorin) 7A	1.50	2.28E-02
Mxd4	Max dimerization protein 4	1.50	4.73E-02
Cmtm6	CKLF-like MARVEL transmembrane domain containing 6	-1.50	3.09E-02
Socs3	suppressor of cytokine signaling 3	-1.52	3.34E-02
Mtm1	X-linked myotubular myopathy gene 1	-1.53	1.43E-02
Mapk12	mitogen-activated protein kinase 12	-1.58	3.98E-02
Zfp317	zinc finger protein 317	-1.63	1.22E-02
Gm6377	predicted gene 6377	-1.68	1.74E-02
Plxnd1	plexin D1	-1.72	1.37E-02
Dmxl1	Dmx-like 1	-1.73	4.38E-02
Pltp	phospholipid transfer protein	-1.86	1.60E-02
Hbb-b1	hemoglobin, beta adult major chain /// hemoglobin, beta adult minor chain /// hemoglobi	-1.91	1.47E-02
Odc1	ornithine decarboxylase, structural 1	-1.94	4.74E-02
1110059E24Rik	RIKEN cDNA 1110059E24 gene	-1.97	2.93E-03
Il5ra	interleukin 5 receptor, alpha	-2.22	1.03E-02
Hba-a1 /// Hba-a2	hemoglobin alpha, adult chain 1 /// hemoglobin alpha, adult chain 2	-2.23	1.10E-02

Table S2. Metabolomic Profiling of WT and VHL bKO B cells, Related to Figure 5

	m/z	RT(Min)	WT1	WT2	WT3	WT CV	KO1	KO2	KO3	KO CV	Ratio (KO/WT)	P Values	VIP		Metabolite group/function	MS mode	Putative ID
M88T34	88.03897	0.573909	15040485	17746861	14244014	0.117123	11332453	7985503	17538884	0.394566	0.783665	0.351938	2.12896		Amino acids	Neg	Beta-Alanine
M118T38	118.0863	0.627532	1.9E+08	1.94E+08	1.77E+08	0.047982	2.51E+08	2.92E+08	2.7E+08	0.07567	1.44644	0.009807	5.69591		Amino acids	Pos	Betaine
M102T37	102.0547	0.611392	25275693	25474590	21554690	0.091611	29121302	25752560	31634556	0.102349	1.196438	0.095502	0.992981		Amino acids	Neg	Dimethylglycine
M175T34	175.1189	0.559648	1.69E+08	1.9E+08	1.63E+08	0.081394	1.97E+08	2.02E+08	1.76E+08	0.07214	1.099377	0.204488	0.499607		Amino acids	Pos	L-Arginine
M132T34	132.029	0.573909	78405857	94760005	72554569	0.140516	63335638	46188319	96056998	0.369729	0.836646	0.470193	4.25393		Amino acids	Neg	L-Aspartic acid
M156T33	156.0768	0.553294	2489467	2465283	2109140	0.090436	3841319	3362430	2997221	0.124495	1.444101	0.032447	0.550356		Amino acids	Pos	L-Histidine
M132T131	132.1018	2.181709	4.33E+08	4.27E+08	3.88E+08	0.059345	5.04E+08	5.36E+08	4.97E+08	0.04056	1.231993	0.007142	4.59876		Amino acids	Pos	L-Isoleucine/leucine
M150T78	150.0584	1.307098	43211223	44008581	40448626	0.0439	56719759	57271395	55851944	0.012639	1.330345	0.002411	1.97256		Amino acids	Pos	L-Methionine
M166T166	166.0862	2.759995	96991274	96989050	87114164	0.060854	1.17E+08	1.25E+08	1.23E+08	0.032079	1.298594	0.003403	2.99334		Amino acids	Pos	L-Phenylalanine
M180T255	180.0656	4.241743	49532101	48332614	40523440	0.106045	62515130	60282672	71332886	0.090295	1.402798	0.014336	2.74404		Amino acids	Pos	Hippuric acid
M116T43	116.0708	0.709387	3.74E+08	3.64E+08	3.28E+08	0.068588	4.09E+08	3.81E+08	4.78E+08	0.118264	1.190598	0.128798	2.35098		Amino acids	Pos	L-Proline
M205T208	205.097	3.469222	16009871	15040716	13508311	0.084919	17714153	19446634	19776598	0.058372	1.277801	0.013553	1.09752		Amino acids	Pos	L-Tryptophan
M182T132	182.0812	2.200994	67813666	69341950	58995153	0.08542	80254566	80908278	83582147	0.021611	1.247739	0.028374	2.01082		Amino acids	Pos	L-Tyrosine
M192T277	192.0655	4.619578	6.11E+08	5.31E+08	4.91E+08	0.111897	3.95E+08	3.67E+08	4.89E+08	0.15353	0.765021	0.066282	14.9488		Amino acids	Neg	Phenylacetylglycine
M146T37	146.0451	0.621344	26475057	25485154	22521511	0.082863	28386325	25934372	34530379	0.149515	1.192925	0.193491	0.831885		Amino acids	Neg	L-Glutamic acid
M147T35	147.0764	0.581182	34607671	39724320	33758588	0.089571	40936896	40694321	47240830	0.086402	1.19226	0.072476	0.788617		Amino acids	Pos	L-Glutamine
M306T92	306.0765	1.535067	6.56E+08	5.93E+08	5.35E+08	0.101722	6.06E+08	5.75E+08	7.4E+08	0.136979	1.076955	0.503152	2.89944		Redox	Neg	Glutathione
M613T131	613.1405	2.178622	922338.9	955795.2	901773.4	0.029425	1329107	968090.3	1494231	0.212912	1.363869	0.160884			Redox	Neg	GSSG
M308T91_1	308.0912	1.515257	2.34E+09	2.3E+09	1.99E+09	0.086248	2.3E+09	2.11E+09	2.41E+09	0.066797	1.027344	0.690607	8.90161		Redox	Pos	Glutathione
M130T112	130.0498	1.870079	50509189	46143315	42071618	0.091252	67201461	63650860	67908494	0.034437	1.432778	0.005016	2.93155		Redox	Pos	Pyroglutamic acid
M133T55	133.013	0.922102	1.09E+08	1.21E+08	69781066	0.267406	83647309	87336059	1.27E+08	0.242374	0.995981	0.985519	1.95529		Energy metabolites	Neg	L-Malic acid
M89T69	89.02298	1.15056	1.5E+08	1.3E+08	1.12E+08	0.14788	1.98E+08	2E+08	2.21E+08	0.061702	1.577171	0.00741	8.31767		Energy metabolites	Neg	L-Lactic acid
M191T107	191.0189	1.787685	78085771	64921782	57678108	0.154659	62875904	63015600	82290275	0.160948	1.037353	0.790388	1.55206		Energy metabolites	Neg	Citric acid
M664T135	664.1184	2.251343	1827002	1704447	1434905	0.121168	4320476	4058094	5492804	0.165218	2.79307	0.01632	1.80662		Energy metabolites	Neg	NADH
M662T126	662.1021	2.104541	2361348	1602052	2311095	0.20302	2216800	3032578	4143389	0.308871	1.496976	0.195281	0.699252		Energy metabolites	Neg	NAD
M784T213	784.1493	3.546638	972928.6	895169	749663.9	0.129881	798052.5	867059.1	1078123	0.159574	1.047932	0.716144	0.165273		Energy metabolites	Neg	FAD
M87T52	87.00743	0.868825	10653309	8616491	8045121	0.150576	11242714	12235712	10612092	0.072031	1.248055	0.084766	0.850488		Energy metabolites	Neg	Pyruvic acid
Manual intgd	145.0142	1.17	1310463	1035680	1238486	0.119249	2028182	2174221	2891213	0.195354	1.978898	0.038567	NA-man intgd		Energy metabolites	Neg	alpha-ketoglutarate
														Acylcarnitine			
M372T61	372.3115	1.018384	8111.621	6297.074	6696.483	0.135532	12318.2	12722.02	13580.7	0.050084	1.829926	0.001636	0.794365	14:0	Acylcarnitine	Pos	Tetradecanoylcarnitine
M398T67	398.3259	1.108536	5691.391	6486.106	5553.47	0.085171	14410.35	9080.054	11655.26	0.227537	1.982163	0.059079	0.710691	16:1	Acylcarnitine	Pos	trans-Hexadec-2-enoyl carnitine
M424T74	424.3419	1.235439	8498.868	6680.521	6953.123	0.132924	18324.85	12720.46	17972.21	0.192106	2.214729	0.02952	0.983129	18:2	Acylcarnitine	Pos	Linoelaidyl carnitine
M400T90	400.3413	1.494315	46850.75	60590.06	38858.46	0.225395	98711	89920.68	80318.08	0.102615	1.838353	0.008453	2.10912	16:0	Acylcarnitine	Pos	L-Palmitoylcarnitine
M426T99	426.3575	1.64539	19705.78	13365.8	17404.9	0.19075	33412.19	29765.79	38463.92	0.128922	2.013649	0.007024	1.35135	18:1	Acylcarnitine	Pos	Oleoylcarnitine
M428T144	428.3728	2.400491	8397.887	6795.744	6152.802	0.162489	10744.02	11490.78	9204.63	0.111238	1.472819	0.02382	0.499965	18:0	Acylcarnitine	Pos	Stearoylcarnitine
Carnitine			1.42E+09	1.42E+09	1.41E+09	0.004133	1.47E+09	1.47E+09	1.87E+09	0.144498	1.130764	0.29998					Carnitine
														Fatty Acid			
M227T97	227.2004	1.617816	260245.3	195789.4	165335.3	**0.233964**	361839	200504.1	229992.5	0.325275	1.275143	0.387387	1.5993	14:0	Fatty acid	Neg	Myristic acid
M253T110	253.2164	1.831265	55234.25	39571.44	71908.27	**0.290996**	148723.8	29897.27	78089.59	0.698437	1.539827	0.479798	1.26464	16:1	Fatty acid	Neg	Palmitoleic acid
M279T125	279.2314	2.08809	525323.1	308254.9	327247.3	**0.310686**	1190870	458078.7	499221.6	0.574975	1.850554	0.298623	6.23585	18:2	Fatty acid	Neg	Linoleic acid
M255T160_2	255.2315	2.672951	5981069	4042799	3778542	**0.261395**	11025479	5087374	5817836	0.442963	1.588903	0.282279	16.9461	16:0	Fatty acid	Neg	Palmitic acid

M331T176	331.2634	2.936205	4477.906	3565.034	4020.894	**0.113505**	6564.542	5432.558	6152.713	0.094703	1.504481	0.00978	0.507138	22:4	Fatty acid		Neg	Adrenic acid
M281T178	281.2473	2.970301	365125.3	225880.7	212791.8	**0.315099**	789192.7	308414.6	338046.5	0.563014	1.786088	0.307161	4.90145	18:1	Fatty acid		Neg	Oleic acid
M307T201	307.2623	3.346671	3263.478	2039.688	1594.801	**0.375809**	7455.321	3206.575	4453.793	0.433437	2.191325	0.150121	0.667356	20:2	Fatty acid		Neg	Eicosadienoic acid
M283T246_2	283.2625	4.09771	10356920	7150666	6626549	**0.251035**	16036844	8729592	9227119	0.360316	1.408526	0.30211	16.4153	18:0	Fatty acid		Neg	Stearic acid
M346T96	346.0549	1.60098	40068216	28703184	25228774	0.247707	61084538	55930830	46889633	0.131521	1.743667	0.019053	4.29376		Nucleotides		Neg	Adenosine monophosphate
M322T58	322.0441	0.965283	5540220	5132608	4687483	0.0833	5895232	5687482	6326644	0.054615	1.16595	0.055768	0.298225		Nucleotides		Neg	Cytidine monophosphate
M323T62	323.0286	1.039659	5170810	5192310	3376372	0.227581	6609577	7844898	6108691	0.130372	1.496647	0.04675	1.25774		Nucleotides		Neg	Uridine 5'-monophosphate
M364T119	364.0656	1.975523	7418829	7407862	4124081	0.300631	12956731	11822992	7747036	0.252698	1.716382	0.086451	1.26562		Nucleotides		Pos	Guanosine monophosphate
M405T45	405.01	0.744113	4628217	3818930	3639996	0.130689	4559925	3989459	5260410	0.138289	1.142519	0.297157	0.059874		Nucleotides		Pos	Uridine 5'-diphosphate
M112T84	112.0508	1.403491	5248502	5063586	3554581	0.201032	4812295	5769500	6316511	0.135168	1.218628	0.221488	0.271615		Nucleotides		Pos	Fragment of cytidine
M152T78	152.0566	1.296892	8837008	16739887	8979963	0.392573	10301753	19571396	72063877	0.980209	2.949835	0.363033	2.46868		Nucleotides		Pos	Guanine
M282T141	282.0842	2.357675	656850.7	679931.5	391163.8	0.278607	1263175	1051711	1075592	0.102474	1.962143	0.010554	0.740506		Nucleotides		Neg	Guanosine
M243T130	243.0617	2.168645	10023642	10296486	6323593	0.249873	7045807	9216400	10544908	0.197674	1.006133	0.975137	0.607749		Nucleotides		Neg	Uridine
M138T43	138.0549	0.717147	19501612	19023653	18243252	0.033568	20654294	19207876	20525002	0.039762	1.063744	0.113967	0.562943		Nicotinamide metabolism		Pos	Trigonelline (N-methylnicotinate)
M197T42	197.0668	0.702239	16272351	14080974	13993354	0.08735	17777570	16175403	19846441	0.102629	1.213155	0.079571	0.56232		Pentose phosphate		Pos	Gluconic acid
M445T43	445.0525	0.714627	35445303	33603884	27731908	0.124871	31462306	28929355	40357674	0.178723	1.041002	0.769283	0.980136		Phospholipid synthesis		Neg	CDP-Ethanolamine
M140T34	140.0105	0.561561	25420291	36687195	24675192	0.232663	25012359	18316571	34297137	0.310147	0.894488	0.641039	2.02566		Phospholipid synthesis		Neg	O-Phosphoethanolamine
M167T108	167.0201	1.793121	6264392	5450392	3296922	0.306419	4683335	5832174	5325159	0.109036	1.055221	0.792216	0.212736		Urea cycle		Neg	Uric acid
M440T216	440.1315	3.602315	408500	323360.4	321521.5	0.141529	476018.8	572755.3	453505.6	0.126523	1.426149	0.034975	0.300505		Vitamins		Neg	Folic acid
M168T127	168.065	2.116604	366674.2	292998.5	272263.6	0.159724	461307.8	564348.7	418256.2	0.155974	1.549368	0.037469	0.354879		Vitamins		Neg	Pyridoxine
M220T177	220.1181	2.947317	59623003	48814973	48594735	0.120444	47425463	46417302	60696683	0.154701	0.984123	0.894539	1.67853		Vitamins		Pos	Pantothenic acid

Transparent methods

Mice

Vhl$^{fl/fl}$ (Stock No: 012933) (Haase et al., 2001), *Hif-1α*$^{fl/fl}$ (Stock No: 007561) (Ryan et al., 2000) and *Cd19*$^{Cre/+}$ (Stock No:006785) (Rickert et al., 1997) mice were purchased from The Jackson Laboratory and used to generate various B cell-specific mutant mice. Mice of 8 to 16 weeks old of both sexes were used and all the animal procedures were approved by Institutional Animal Care and Use Committee of Agency for Science, Technology and Research.

Flow cytometry analysis

Single-cell suspensions were prepared from BM, spleen, inguinal lymph nodes and peritoneal cavities of mice and stained with biotin- or fluorescent-labelled antibodies and subjected to flow cytometry analysis as described previously (Xu et al., 2015). mPTP opening was labelled with mPTP staining dye (Biovision) following the manufacturer's instruction and analysed by flow cytometry. Data were collected on a LSR II flow cytometer (BD Pharmingen) and analyzed with Flowjo (Treestar). The following antibody clones were purchased from BD Pharmingen or as specified: anti-CD3 (145.2C11), anti-CD5(53-7.3), anti-CD19(1D3), anti-CD21(7G6), anti-CD23(B3B4), anti-CD25(PC61), anti-CD43 (S7), anti-CD69 (H1.2F3), anti-CD80 (16-10A1), anti-CD86 (GL-1), anti-CD93 (AA4.1), anti-IgM(R6-60.2), anti-IgD (11-26C.2a), anti-B220 (RA3-6B2), anti-MHC II (M5/114.15.2), anti-Ki67 (B56). Dead cells were excluded by DAPI (Sigma) staining. To assess mPTP status in B cells, splenic B cells were equilibrated in RPMI1640 complete medium [RPMI + 10% FBS + 1x penicillin-streptomycin + 1mM sodium pyruvate + 2 mM L-Glutamine + 1x minimum essential medium (MEM) with non-essential amino acids + 50 μM b-mercaptoethanol] for 2 hr and labelled with mPTP staining dye (Biovision) followed by flow cytometry analysis. For cell sorting, pro-B ($IgM^-B220^+CD43^+$), pre-B ($IgM^-B220^+CD43^-$), immature B (IgM^+IgD^-) and mature B (IgM^+IgD^+) cells from BM and total B (IgM^+B220^+) cells from spleen were purified by fluorescence-activated cell sorting on a FACSAria cell sorter (BD Pharmingen). Naïve B cells were purified from spleen with anti-CD43 mAb-coupled magnetic beads using magnetic-activated cell sorting (MACS) negative selection protocol (Miltenyl Biotech, Bergisch Gladbach, Germany).

In vitro B cell proliferation and survival

Naïve B cells were purified from spleen with anti-CD43 mAb-coupled magnetic beads using magnetic activated cell sorting negative selection protocol (Miltenyl Biotech, Bergisch

Gladbach, Germany). To measure cell proliferation, naïve B cells were labelled with 1 μM CellTrace™ CFSE dye (ThermoFisher Scientific) and cultured in complete RPMI1640 medium alone or with 1μg/ml LPS (Sigma), 10 μg/ml anti-IgM (Jackson Laboratory) or 1 μg/ml anti-CD40 (BD Pharmingen) antibodies for 24 hours at 37 $^{\circ}$C. The dilution of CFSE in B cells was measured by flow cytometry. To examine cell survival, B cells were cultured in RPMI 1640 medium alone or treated with 100 ng/ml LPS, 10 μg/ml anti-IgM or 1 μg/ml anti-CD40 antibodies for 16 hours at 37 $^{\circ}$C. Cell survival was determined by flow cytometry using Annexin V Apoptosis Detection Kit (BD Pharmingen) and showed as percentage of Annexin V^- PI^- live cells.

Quantitative RT-PCR and microarray

Total RNA was prepared from various sorted B cell populations using TRIzol (Invitrogen) and subjected to cDNA synthesis with reverse-transcriptase using random hexamers as primers (Research Instruments) followed by quantitative real-time PCR analysis using platinum SYBR Green Supermix (Life Technologies). For microarray study, total RNA was subjected to DNase I digestion using RNase-Free DNase Set and RNeasy MinElute Cleanup Kit (Qiagen), and cRNA was prepared and hybridized on Affymetrix GeneChip® Mouse Genome 430 2.0 arrays (ThermoFisher Scientific) using standard Affymetrix protocol. The significantly differentially regulated genes were detected using Partek Genomics Suite (PGS) software (Partek Inc.). A list of HIF-1α and HIF-2α target genes was collated from Ingenuity Knowledge Base and "HIF-1-alpha transcription factor network" and "HIF-2-alpha transcription factor network" entries in Pathway Interaction Database. Significantly differentially expressed HIF-1α target genes were determined using GSEA by uploading the RMA-normalized microarray expression values generated from PGS, and using the difference of classes as the metric for ranking genes and gene set as permutation type.

Immunofluorescence histology

Spleens were harvested and embedded in Tissue-Tek O.C.T. (Sakura) and "snap-frozen" in dry ice and ethanol and stored at −80°C as described previously (Xu et al., 2015). Splenic sections of 8 μm in thickness were prepared, air-dried and fixed in ice-cold acetone for 15 minutes. After blocking with 5% rat serum, sections were stained at room temperature for 30 min with a cocktail of antibodies from BD Pharmingen or as specified: anti-CD3 (145-

2C11), anti-IgD (11-26C.2a), IgM (R6-60.2) anti-F4/80 (BM8, Biolegend), anti-CD169 (Moma-1 Abcam). Streptavidin-APC (BD, Pharmingen) were used in a second step to detect biotinylated antibodies. After washing, sections were mounted with CYTOSEAL 60 (Electron Microscopy Sciences) and analysed on a FV1000 confocal microscope (Olympus) using 4x or 20× objectives. Images were acquired with Olympus Fluoview Version 2.1 software.

Immunoblotting and protein palmitoylation detection

Sample preparation and immunoblotting were performed as described previously (Huo et al., 2010). Briefly, whole-cell lysate from B cells were prepared using lysis buffer (10 mM Tris-HCl, pH 8.0, 150 mM NaCl, 1 mM EDTA, 1% Igepal CA-630, 0.2 mM Na3VO4 and a protease inhibitor cocktail (Roche, Basel, Switzerland)) Protein concentrations were determined and equal amount of proteins was loaded and separated by SDS-PAGE, transferred to PVDF (polyvinylidene difluoride) membranes and blotted with specific monoclonal or polyclonal antibodies. β-actin was used as loading control. Antibodies were from Cell Signalling: anti-VHL (2378s), anti-HK1 (C35C4), anti-HK2 (C64G5), anti-PFKP (D4B2); anti-PFKFB2 (D7G5R), anti-ALDO (D73H4), anti-GAPDH (D16H11), anti-PGAMI (D3J9T), anti-ENO1, PKM1 (C103A3), anti-PKM2 (D78A4), anti-LDHa (C4B5), anti-PDH (C54G1), anti-PDK (C47H1), anti-caspase-8 (D35G2), anti-HIF-2α (D9E3), anti-PFKL, anti-ENO1 and anti-caspase-9; or from Santa Cruz: anti-Fas (A-20), anti-FADD (H-181) and anti-β-Actin, or from Abcam: anti-BNIP3 (EPR4034) and anti-BNIP3L (EPR4033); or from Cayman: anti-HIF-1α.

For Fas palmitoylation detection in B cells, an acyl/biotinyl exchange (ABE) protocol was adapted from previous studies (Wan et al., 2007; Drisdel and Green, 2004). Briefly, 1×10^7 purified splenic B cells from WT and VHL bKO B cells were equilibrated in complete RPMI1640 medium for 2hr and homogenized in lysis buffer (150 mM NaCl, 50 mM Tris, 5 mM EDTA, 10 mM N-ethylmaleimide, protease inhibitors including 250 μg/L each of pepstatin, leupeptin, antipain and chymostatin, pH 7.4). Total membrane proteins were collected by high-speed centrifugation, followed by three steps of ABE chemical reaction: (1) membrane protein lysates were re-suspended in lysis buffer (1.7% Triton X-100, 150 mM NaCl, 50 mM Tris, 5 mM EDTA, protease inhibitors, pH 7.4) with 10 mM N-ethylmaleimide to block free thiol groups; (2) proteins were precipitated with chloroform-methanol and

resuspended in 0.7 M hydroxylamine, which cleaves cysteine-palmitoyl thioester linkages; and (3) the newly exposed thiols were labelled with 1 mM biotin-HPDP (biotin-HPDP-N-[6-(biotinamino)hexyl]-3'-(2'-pyridyldithio) propionamide. After removal of unreacted HPDP–biotin by chloroform-methanol precipitation, biotinylated proteins were affinity-purified using streptavidin-agarose and subjected to SDS-PAGE and probed with anti-Fas antibody. Specificity of the ABE reaction was controlled by samples without hydroxylamine treatment.

Metabolism assays

For real-time analysis of OCR and ECAR, purified splenic B cells were measured with a XF-96 Extracellular Flux Analyzer (Agilent). First, B cells ($3x10^5$/well) were seeded in Cell-Tak (Corning) coated plates. Glycolysis, basal OCR and Spare Respiratory Capacity (SRC) of B cells were determined according to the manual of Seahorse XF Glycolysis Stress Test or Cell Mito Stress Test kits (Agilent) using the following concentrations of injected compounds as indicated: glucose, 10 mM; 2-DG, 50 μM, oligomycin ,1 μM; fluorocarbonyl cyanide phenylhydrazone (FCCP), 1 μM; rotenone/antimycin A, 0.75 μM and etomoxir, 200 μM. The levels of lactate, citrate, α-ketoglutarate and pyruvate dehydrogenase activity in B cells were measured using different assay kits from Sigma according to manufacturer's instructions.

Mass spectrometry and carbon tracing

For global metabolite profiling of B cells, metabolites were extracted using two-phase liquid-liquid extraction protocol and subjected to liquid chromatography-mass spectrometry (LC-MS). Intracellular metabolites were first extracted using two-phase liquid-liquid extraction protocol as previously described (Huo et al., 2016) and stored at -80^{o}C and reconstituted in respective chromatography solvents prior to analysis. The polar metabolites were analyzed by LC-MS using an ACQUITY UPLC system (Waters, MA, USA) in tandem with a mass spectrometer (QExactive, Thermo, MA, USA). The UPLC method was based on the use of a reversed phase column with polar encapping (Acquity HSS T3, Waters). Electrospray ionization (ESI) was conducted in both positive and negative modes with mass range of 70 to 1050 m/z at a resolution of 70,000. Sheath and auxiliary gas flow was set at 30.0 and 20.0 (arbitrary units) respectively, while a capillary temperature of 400^{o}C was used. The spray voltage was 1.5kV and 1.25 kV respectively, for positive and negative mode ionization. All

raw LC-MS data obtained were pre-processed using XCMS peak finding algorithm (AC) and normalized to total protein concentration in each sample.

For isotopic carbon tracing study, $2x10^7$ VHL bKO and control B cells were first incubated in complete RPMI medium containing 2 mM [$^{13}C_5$,$^{15}N_2$] glutamine (Cambridge Isotope Laboratories, Inc) for 4 h. Intracellular metabolites were subsequently extracted using two-phase liquid-liquid extraction protocol and subjected to liquid chromatography-mass spectrometry (LC-MS) as described above. Raw data was processed and peak integration was performed using TraceFinder v3.3 (Thermo). Mass isotopomer distributions were corrected for natural isotope abundance (Fernandez et al., 1996; Trefely et al., 2016).

Statistical analysis

Statistical analyses were performed with a two-tailed unpaired or a two-tailed paired Student's *t*-test using Graphpad Prism software (version 7). Difference between experimental and control groups were considered significant when *P* values were below 0.05. *p* value: ns, not significant; *p,0.05; **p,0.01 and ***p,0.001.

Supplemental References

Drisdel,R.C. and Green,W.N. (2004). Labeling and quantifying sites of protein palmitoylation. Biotechniques *36*, 276-285.

Fernandez,C.A., Des,R.C., Previs,S.F., David,F., and Brunengraber,H. (1996). Correction of 13C mass isotopomer distributions for natural stable isotope abundance. J. Mass Spectrom. *31*, 255-262.

Haase,V.H., Glickman,J.N., Socolovsky,M., and Jaenisch,R. (2001). Vascular tumors in livers with targeted inactivation of the von Hippel-Lindau tumor suppressor. Proc. Natl. Acad. Sci. U. S. A *98*, 1583-1588.

Huo,J., Ma,Y., Liu,J.J., Ho,Y.S., Liu,S., Soh,L.Y., Chen,S., Xu,S., Han,W., Hong,A., Lim,S.C., and Lam,K.P. (2016). Loss of Fas apoptosis inhibitory molecule leads to spontaneous obesity and hepatosteatosis. Cell Death. Dis. *7*, e2091.

Huo,J., Xu,S., and Lam,K.P. (2010). Fas apoptosis inhibitory molecule regulates T cell receptor-mediated apoptosis of thymocytes by modulating Akt activation and Nur77 expression. J. Biol. Chem. *285*, 11827-11835.

Rickert,R.C., Roes,J., and Rajewsky,K. (1997). B lymphocyte-specific, Cre-mediated mutagenesis in mice. Nucleic Acids Res. *25*, 1317-1318.

Ryan,H.E., Poloni,M., McNulty,W., Elson,D., Gassmann,M., Arbeit,J.M., and Johnson,R.S. (2000). Hypoxia-inducible factor-1alpha is a positive factor in solid tumor growth. Cancer Res. *60*, 4010-4015.

Trefely,S., Ashwell,P., and Snyder,N.W. (2016). FluxFix: automatic isotopologue normalization for metabolic tracer analysis. BMC. Bioinformatics. *17*, 485.

Wan,J., Roth,A.F., Bailey,A.O., and Davis,N.G. (2007). Palmitoylated proteins: purification and identification. Nat. Protoc. *2*, 1573-1584.

Xu,S., Ou,X., Huo,J., Lim,K., Huang,Y., Chee,S., and Lam,K.P. (2015). Mir-17-92 regulates bone marrow homing of plasma cells and production of immunoglobulin G2c. Nat. Commun. *6*, 6764.